Google Earth Engine Cloud Computing Platform for Remote Sensing Big Data Applications: A Comprehensive Review

Meisam Amani, *Senior Member, IEEE*, Arsalan Ghorbanian, Seyed Ali Ahmadi, Mohammad Kakooei, Armin Moghimi, S. Mohammad Mirmazloumi, *Student Member, IEEE*, Sayyed Hamed Alizadeh Moghaddam, Sahel Mahdavi, Masoud Ghahremanloo, Saeid Parsian, Qiusheng Wu, and Brian Brisco

***Abstract*—Remote sensing (RS) systems have been collecting massive volumes of datasets for decades, managing and analyzing of which are not practical using common software packages and desktop computing resources. In this regard, Google has developed a cloud computing platform, called Google Earth Engine (GEE), to effectively address the challenges of big data analysis. In particular, this platform facilitates processing big geo data over large areas and monitoring the environment for long periods of time. Although this platform was launched in 2010 and has proved its high potential for different applications, it has not been fully investigated and utilized for RS applications until recent years. Therefore, this study aims to comprehensively explore different aspects of the GEE platform, including its datasets, functions, advantages/limitations, and various applications. For this purpose, 450 journal articles published in 150 journals between January 2010 and May 2020 were studied. It was observed that Landsat and Sentinel datasets were extensively utilized by GEE users. Moreover, supervised machine learning algorithms, such as Random Forest, were more widely applied to image classification tasks. GEE has also been employed in a broad range of applications, such as Land Cover/land Use classification, hydrology, urban planning, natural disaster, climate analyses, and image processing. It was generally observed that the number of GEE publications have significantly increased during the past few years, and it is expected that GEE will be utilized by more users from different fields to resolve their big data processing challenges.**

***Index Terms*—Big data, cloud computing, Google Earth Engine (GEE), remote sensing (RS).**

Manuscript received June 7, 2020; revised July 18, 2020 and August 11, 2020; accepted August 26, 2020. Date of publication September 1, 2020; date of current version September 17, 2020. *(Corresponding author: Meisam Amani.)*

Meisam Amani and Sahel Mahdavi are with the Wood Environment & Infrastructure Solutions, Ottawa, ON K2E 7L5, Canada (e-mail: meisam.amani@woodplc.com; sahel.mahdavi@woodplc.com).

Arsalan Ghorbanian, Seyed Ali Ahmadi, Armin Moghimi, and Sayyed Hamed Alizadeh Moghaddam are with the Faculty of Geodesy and Geomatics Engineering, Department of Remote Sensing and Photogrammetry, K. N. Toosi University of Technology, Tehran 1996715433, Iran (e-mail: a.ghorbanian@email.kntu.ac.ir; cpt.ahmadisnipiol@yahoo.com; moghimi.armin@gmail.com; h.alizadeh@email.kntu.ac.ir).

Mohammad Kakooei is with the Department of Electronic Engineering, Babol Noshirvani University of Technology, Babol 4714871167, Iran (e-mail: kakooei.mohammad@stu.nit.ac.ir).

S. Mohammad Mirmazloumi is with the Centre Tecnològic de Telecomunicacions de Catalunya (CTTC/CERCA), 08860 Castelldefels, Spain (e-mail: sm.mirmazloumi@cttc.es).

Masoud Ghahremanloo is with the Department of Earth and Atmospheric Sciences, University of Houston, Houston, TX 77004 USA (e-mail: mghahremanloo@uh.edu).

Saeid Parsian is with the Department of Surveying Engineering, Tafresh University, Tafresh 395187611, Iran (e-mail: saeid90parsian@gmail.com).

Qiusheng Wu is with the Department of Geography, University of Tennessee, Knoxville, TN 37996 USA (e-mail: qwu18@utk.edu).

Brian Brisco is with the Canada Center for Mapping and Earth Observation, Ottawa, ON K1S 5K2, Canada (e-mail: brian.brisco@canada.ca).

Digital Object Identifier 10.1109/JSTARS.2020.3021052

I. Introduction

In RECENT years, there has been a significant increase in the number of remote sensing (RS) datasets acquired by various spaceborne and airborne sensors with different characteristics (e.g., spectral, spatial, temporal, and radiometric resolutions) [1]. This trend is expected to continue due to the availability of more open-access RS datasets and daily advancement in sensor, image processing, and computer vision technologies [2].

Working with petabytes of RS datasets is a challenging task and has its own special requirements. The challenges of big data processing and analyzing can be divided into two categories: common and individual facets [3]. The common challenges are more related to handling big data and include big data computing, big data collaboration, and big data methodologies. The individual challenges are related to big data life cycle in different applications, such as the appropriate data identification, data deployment, data representation, data fusion, as well as data visualization and interpretation. In order to provide a comprehensive solution that can meet a wide range of current and future challenges and requirements in RS applications, one of the most important steps is to develop a safe, efficient, and advanced cloud computing platform [3], [4].

Cloud computing platforms are efficient ways of storing, accessing, and analyzing datasets on very powerful servers, which virtualize supercomputers for the user. These systems provide infrastructure, platform, storage services, and software packages in a variety of ways for the customers [3], [4]. Several cloud computing platforms have so far been developed. For example, Amazon Web Services (AWS) is a pay-as-you-go platform, where users pay based on the hours that they use the services [2]. AWS has a dedicated cloud Earth Observation (EO) offering called "Earth on AWS" as part of its Public Dataset Program, which includes open data from several satellites such

This work is licensed under a Creative Commons Attribution 4.0 License. For more information, see https://creativecommons.org/licenses/by/4.0/

as Landsat-8, Sentinel-1, Sentinel-2, China–Brazil Earth Resources Satellite program, National Oceanographic, and Atmospheric Administration Advanced (NOAA) image datasets, as well as global model outputs. AWS also hosts open data supplied by DigitalGlobe with its SpaceNet challenges. Moreover, AWS hosts the largest suite of machine learning services [4]. Azure is another cloud computing platform hosted by Microsoft. This platform has established the Artificial Intelligence (AI) for earth initiative to facilitate the use of its AI tools for addressing environmental challenges in four main areas of climate, agriculture, biodiversity, and water. Azure only contains Landsat and Sentinel-2 products for North America, since 2013, as well as moderate resolution imaging spectroradiometer (MODIS) imagery. Azure is also a pay-as-you-go platform which provides virtual systems for the users [5].

Google Earth Engine (GEE) is another cloud computing platform which was launched by Google, in 2010. GEE uses Google's computational infrastructure and available open-access RS datasets [6]. GEE is the most popular big geo data processing platform, facilitating the scientific discovery process by providing users with free access to numerous remotely sensed datasets [1], [2]. Users can access GEE via an internet-based Application Programming Interface (API) and a web-based Interactive Development Environment [2], [6]. Additionally, users do not need to have expertise in web programming or HyperText Markup Language to use GEE for different applications [6]. GEE has the features of an automatic parallel processing and fast computational platform to effectively deal with the challenges of big data processing [6], [7]. For instance, according to Hansen *et al*. [8], it only took 100 h to process 654 178 Landsat-7 images (about 707 terabytes) within GEE and produce a global map of forests. This was reported as a great achievement because if they did not use GEE, this process would have taken a million hours to complete. Furthermore, users do not need to download the available dataset within GEE in order to use them or install any software to perform the processing tasks existing in GEE. However, GEE users can utilize complementary software packages or process their own private datasets within this platform. This platform also contains various built-in algorithms, such as classification algorithms, to analyze data at a planetary scale and also helps scientists to develop their own algorithms with less effort than before [1], [2], [9].

As discussed, the remarkable capabilities of GEE provide unprecedented opportunities to employ this platform for big data processing and interpretation and, therefore, it is effectively employed in a broad variety of disciplines in all branches of Earth science studies. It is also expected that users will more frequently use this cloud computing service considering the trends of GEE studies in recent years. There are currently four GEE literature review studies conducted by Gorelick *et al.* [6], Kumar and Mutanga [9], Mutanga and Kumar [10], and Tamiminia *et al.* [2], published between 2017 and 2020, respectively. Gorelick *et al.* [6] was the first comprehensive GEE review paper conducted by the main GEE developers. The authors comprehensively discussed different aspects of GEE, including data catalog, system architecture, functions, data distribution models, efficiency, along with several applications and challenges. Kumar and Mutanga [9] also briefly discussed the publication and authorship trends, datasets, study areas, and applications of GEE by reviewing 300 journal papers. Furthermore, Mutanga and Kumar [10] briefly discussed four main applications of GEE. More recently, Tamiminia *et al.* [2] also discussed various aspects of GEE by reviewing 349 journal papers. The authors provided comprehensive information about the GEE publications based on study areas, number of publications, datasets and products, functions, sensor type and resolutions, classification accuracies, and various applications.

There is still need for a more comprehensive review to discuss various aspects of the GEE platform. Therefore, in this study, 450 journal articles along with peer-reviewed conference papers were investigated through eight main sections: Section I provides an introduction to GEE; Section II provides an overview of the GEE platform; Section III presents different datasets included in this platform; Section IV discusses various GEE functions and algorithms; Section V provides comprehensive information about the advantages and limitations of GEE; Section VI analyzes the pattern of GEE publications over one decade; Section VII discusses different applications of GEE; and finally Section VIII provides several case studies, in which GEE was applied to process and analyze big data over large areas and within a long period of time.

II. GEE Platform Overview

GEE is mainly composed of the following three platforms:

1) Earth Engine (EE) Explorer;
2) EE Code Editor;
3) EE Timelapse.

The details of each platform are discussed in the following sections.

A. EE Explorer

EE Explorer (see Fig. 1) is a data viewer platform which allows users to access the massive datasets available in the EE Data Catalog. The Data Catalog houses millions of publicly available datasets, including a complete series of Landsat-4, -5, -7, and -8, MODIS, Sentinel-1, -2, -3, and -5P imagery, as well as several atmospheric, meteorological, and vector datasets, which will be further discussed in Section III. The Data Catalog receives approximately 4000 new datasets every day [11].

As illustrated in Fig. 1, the EE Explorer is composed of the Workspace [see Fig. 1(a)] and the Data Catalog [see Fig. 1 (b)]. In the Data Catalog, users can search among massive datasets and import them to the Workspace. In the Workspace, users can manage and visualize datasets. The Workspace also enables users for a quick view, zoom, and pan. Additionally, it allows users to set parameters related to the visualization setting, such as contrast, brightness, and opacity levels. To better inspect any changes over time, users can add multiple layers to the Workspace. Users can display the layers in a three-band RGB or a single-band grayscale/pseudocolor representation [6]. For example, Fig. 1(a) demonstrates a true color composite of a MODIS bidirectional reflectance distribution function (BRDF)-adjusted image.

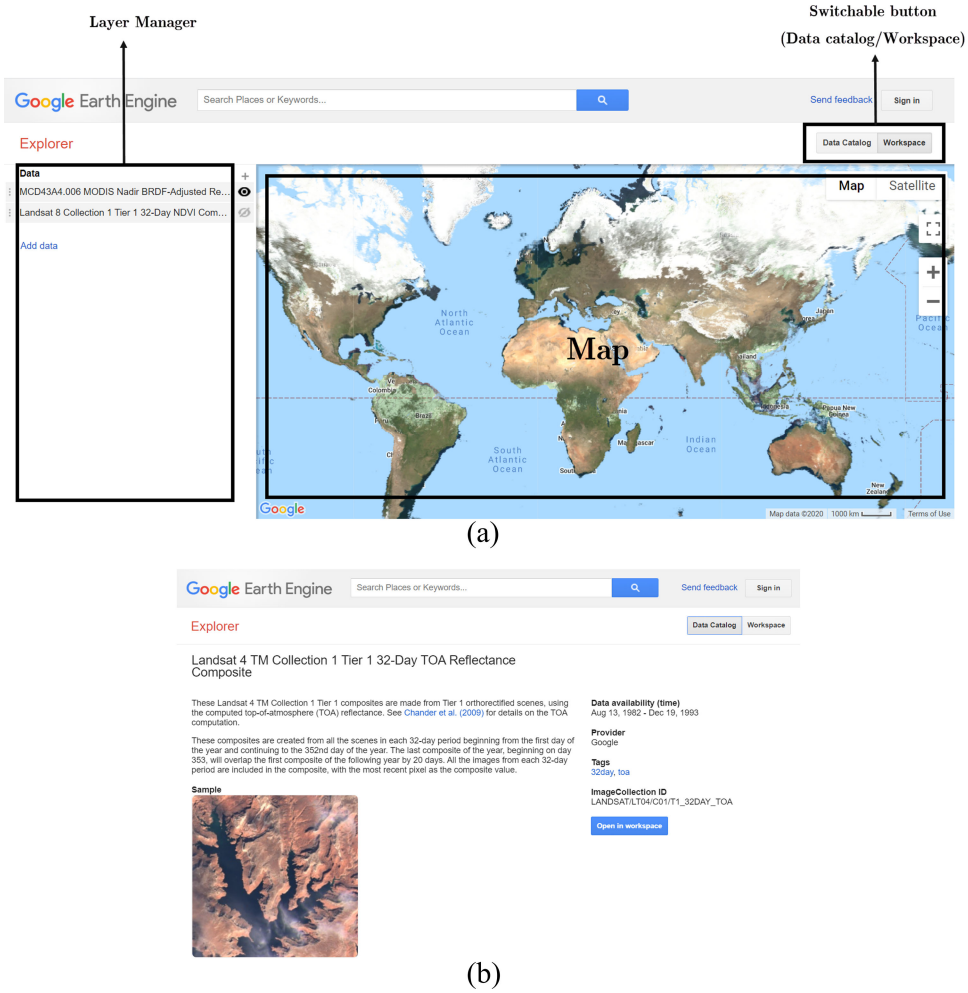

Fig. 1. Earth Engine Explorer platform. (a) Workspace. (b) Data Catalog.

B. EE Code Editor

While the EE Explorer platform is designed to visualize datasets, the EE Code Editor (see Fig. 2) is designated to process big data using a JavaScript programming language and to develop EE applications. According to Fig. 2, the EE Code Editor is composed of the following elements: Code editor, Map, Layer manager, Geometry tools, and several tabs, including Script, Doc, Assets, Inspector, Console, and Tasks.

The central panel allows users to write their JavaScript code. GEE processes the written codes and illustrates the results as images in the Map panel or as messages in the Console Tab. Similar to the EE Explorer, users can set the visualization parameters via the Layer manager in the Code Editor (see Fig. 2). In the Script tab, numerous examples of scripts facilitate developing applications. There are more than 800 prebuilt functions (discussed in detail in Section IV) in the EE library, users can become familiar with them using the Doc tab, providing API reference documentation [6].

As previously mentioned, GEE includes big open-access datasets. Users, however, are not restricted to use only these datasets. They can upload and manage their own data using the Asset tab. It is also possible to interactively query the map using the Inspector tab. Finally, the Geometry tools allow users to draw geometric features, such as points, lines, and polygons, which can be used in further analyses [6].

C. EE Time-Lapse

GEE combines petabytes of RS datasets over four decades and produces a global, zoomable, and cloud-free video over space and time in its EE Time-laps platform [6]. The Timelapse platform is an example of the great computational power of the GEE platform. This platform provides the most comprehensive picture of the Earth revealing how its residents are treating it. For instance, through EE Time-lapse, one can easily observe the fast retreat of Mendenhall Glacier in Alaska, decapitation of West Virginia Mountains by the mining industry, forest loss in the Amazon, and drying Urmia lake in Iran over time.

III. GEE Datasets

As discussed, GEE contains an immense number of datasets, including raw datasets, preprocessed data, elevation models, and

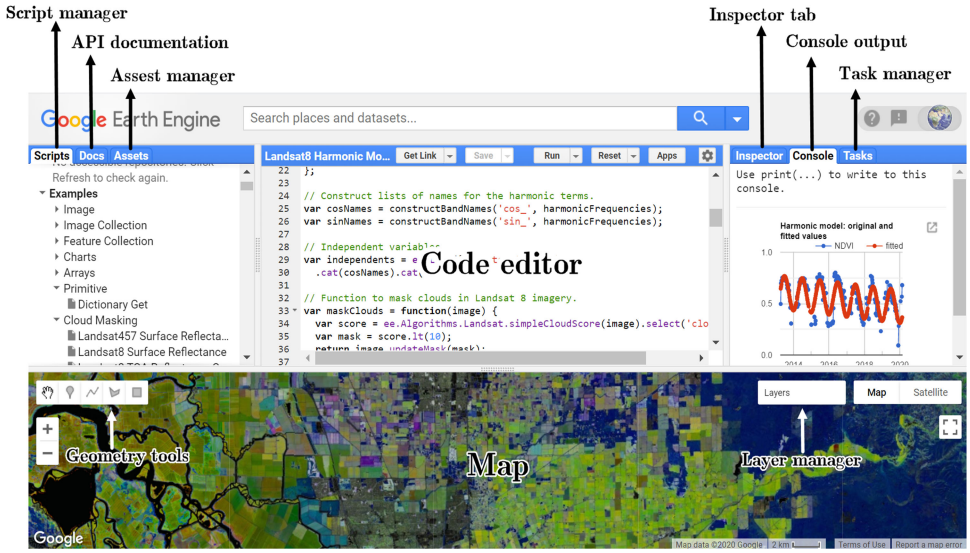

Fig. 2. Overview of the Earth Engine Code Editor.

products at global, national, and regional extents. Table IV in the Appendix provides all available datasets within GEE along with a brief description of each. Some of these datasets, which are frequently utilized by users are discussed in more detail in the following.

Landsat datasets are valuable resources to perform temporal analysis. Landsat collection includes seven multispectral satellites: Landsat 1–3 (1972–1983), Landsat-4 (1982–1993), Landsat-5 (1984–2012), Landsat-7 (1999–present), and Landsat-8 (2013–present). Landsat satellites have optical sensors, the images of which may be obscured by clouds. Therefore, temporal cloud detecting, masking, and removing are essential preprocessing steps in different applications, such as image classifications using multitemporal imagery [12]. Additionally, the availability of the multitemporal Landsat datasets has facilitated national and global scale analysis [13]. Landsat-based datasets within GEE have been employed in various applications. For instance, Landsat data available in GEE have been widely utilized in generating Land Cover/Land Use (LCLU) maps (e.g., [14]–[16]). Moreover, urban detection and extraction is an important task in the economic investigation due to rapid population growth. Therefore, several studies have utilized Landsat data in urban monitoring [17], [18].

GEE includes datasets acquired by Sentinel satellites, developed by the European Space Agency (ESA). Sentinel collection includes Sentinel-1 Synthetic Aperture RADAR (SAR) (2014–present), Sentinel-2 multispectral (2015–present), Sentinel-3 Ocean and Land Color (2016–present), and Sentinel-5P Tropospheric Monitoring (2018–present) datasets. Sentinel-1 and Sentinel-2 have been extensively utilized by GEE users for different applications. Their 10 m spatial resolution makes it possible to analyze objects in a better resolution compared to Landsat images. They can also simplify the procedure of training and validation steps in image classification tasks. Mandal *et al.* [19] applied Sentinel-1 SAR data to map rice and monitor its temporal changes. Additionally, Traganos *et al.* [20] estimated satellite-derived bathymetry (SDB) of three regions in the Aegean Sea using Sentinel-2 time-series analysis.

GEE includes MODIS images. MODIS has a great potential in near-real-time (NRT) mapping of the ground surface in national and global scales. MODIS acquires images in 36 spectral bands, the spatial resolutions of which vary from 250 m to 1 km. MODIS time series are available in GEE Data Catalog from 2000 to present, facilitating temporal analysis over globe. Campos-Taberner *et al.* [21] developed a temporal investigation on MODIS-based indices, including the global Leaf Area Index, Canopy water content, Fraction Vegetation Cover, and Fraction of Absorbed Photosynthetically Active Radiation.

IV. GEE Functions

GEE provides various functions to perform spectral and spatial operations on either a single image or a batch of images. Different operations within the GEE platform, ranging from simple mathematical operations to advanced image processing and machine learning algorithms are illustrated in Fig. 3. Various pixel-based spectral operations, which have high potential to be implemented in parallel on cloud architecture, are included in GEE. However, GEE supports fewer spatial functions, such as Gaussian and Laplacian filters, edge detection methods (e.g., Sobel, Roberts, and Canny), line detection via the Hough Transform, and morphological operators (e.g., dilation and erosion) due to parallel implementation issues. Moreover, GEE currently does not support several functions, including frequency domain algorithms (e.g., FFT and Wavelet), hierarchical algorithms (e.g., hierarchical clustering), graph-based methods (e.g., graphcut), geometric descriptors (e.g., Haar, SIFT, SURF), and physical-based models (e.g., radiative transfer models).

Both supervised and unsupervised machine learning algorithms are accessible through the GEE library. For example, the classification and regression tree (CART), support vector machine (SVM), and random forest (RF) classifiers are among

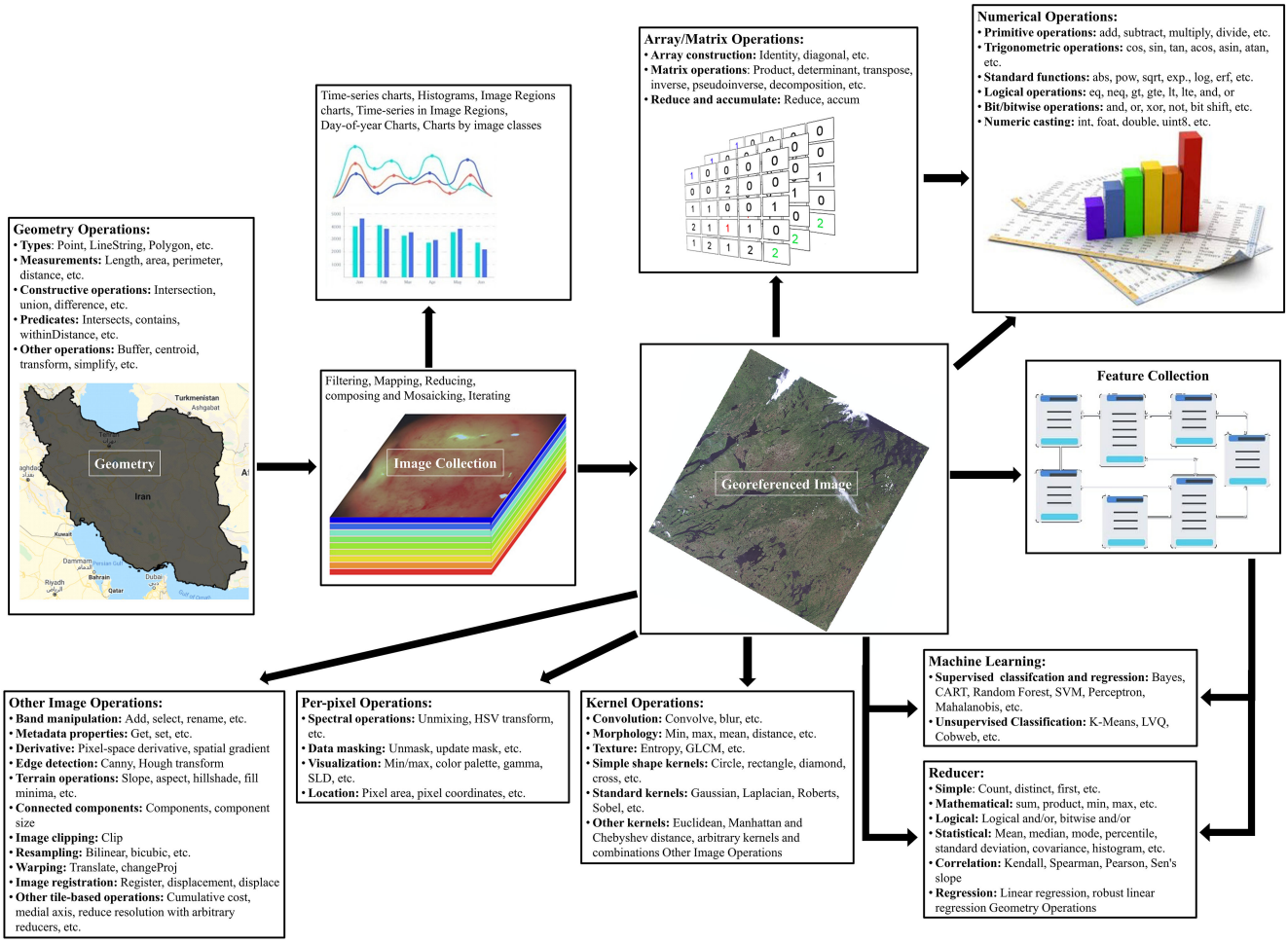

Fig. 3. Overview of different supporting functions within GEE.

the supervised classification algorithms within GEE. Labeled samples are required in supervised classification methods to train the classifiers, for which both sampling and training functions are available in GEE. There are also many clustering algorithms in GEE, such as *K*-means. *K*-means is a popular clustering method in the data mining area. The algorithm requires users to define the number of clusters (*K*) and the stopping criteria [22]–[24]. Besides the original *K*-means, two modified versions of *K*-means (i.e., Cascade *K*-means [25] and *X*-means [26]), in which the number of clusters is estimated automatically, are available in GEE. Cobweb is another clustering algorithm which hierarchically handles data instances data instances. It constructs a classification tree and manages it through merging and splitting steps [27]. Simple noniterative clustering (SNIC) is another clustering-based segmentation method, which is initiated with randomly/manually determined seeds and generates segments [28]. SNIC is widely utilized by users to perform object-based image classifications (e.g., [29]).

As mentioned before, GEE contains over 40 years of datasets, facilitating temporal and change analyses. For temporal analysis purposes, several functions, such as continuous change detection and classification (CCDC) [30], exponentially weighted moving average change detection (EWMACD) [31], and Landsat-based detection of Trends (LandTrendr) [32] are available. CCDC fits harmonic functions to temporal data to detect points with significant variations. EWMACD calculates a model according to the training data. Then, the difference between the model and real data points are found according to the Shewhart X-bar charts and an exponentially weighted moving average. LandTrendr is specially designed for Landsat data and finds the pixel-based spectral change in temporal analysis. Vegetation analysis is also a popular subject in temporal analysis. Therefore, GEE has several algorithms, such as vegetation change tracker (VCT) [33] and vegetation regeneration and disturbance estimates through time (VERDET) [34], which are specifically developed for this purpose. VCT can automatically analyze Landsat time-series images to generate forest disturbance history. VERDET categorizes forest change into three types, including disturbed, stable, and regenerating. The analysis is based on the total variation regularization in the spatial and temporal domain [34].

V. GEE Advantages and Limitations

GEE is a valuable tool in analyzing geospatial data that provides many capabilities for researchers, especially for the RS community. However, there are also several limitations that users

TABLE I
MAIN ADVANTAGES OF GEE BIG GEO DATA PROCESSING PLATFORM

	Advantages	Limitations
Cloud Infrastructure	• Free for research, educational, and nonprofit use • Uses Google power • Parallel processing • Optimized for geospatial data analysis • Capable of processing peta-byte scale data • Data are available online for all users • sharable codes and scripts • No need to install 3rd party software • Uses image pyramids and tiles to enhance processes • Fast filtering and sorting of data	• Training machine/deep learning algorithms is limited to only 100 MB of data • More features mean fewer pixels • Visualizing large spatial extents may result in slowdowns or breaks • Writing code requires knowledge in server-side • Translating all techniques to server-side understandable functions not always easy • Debugging is relatively challenging • Paid license for commercial applications
API	• Web-based interface • Uses JavaScript and Python • Online IDE to run and debug codes • Similar to existing open-access components • Easy access from within Google Colab Jupyter notebooks	• JavaScript and Python codes are run on client-side • Client-side functions run on the user's browser • Users browsers' capabilities are limited to their systems' capabilities
Data	• Large catalog of datasets • Archived data from over 40 years • Near-real-time data uploaded daily • Capability of uploading data by users • Capability of downloading the results anytime • Automatically handles data projection • Most data have been already preprocessed and corrected • Multiple derivative products are already available	• Limited to 250 GBs of user data upload • Downloading data depends on user's internet quality and data volume • New data require extensive time (e.g., one month) to be corrected and preprocessed • Complex SAR amplitude and phase are not stored • Data is mainly not private
Functions	• Large set of callable functions, • Expanding the library of methods and packages • Parallel-in-nature algorithms • Contains machine learning, image processing, vector processing, geometrical analysis, visualization algorithms • Availability of tutorials and documentations for algorithms	• Only hosts some selected data mining models • Image analysis is restricted to existing tools • Developing new tools is not easy • There are not enough atmospheric correction algorithms

should be aware of. The key advantages and limitations of GEE are summarized in Table I and discussed in more detail in the following section. As illustrated in Table I, the advantages and disadvantages of GEE are investigated within the four categories of cloud infrastructure, API, data, and functions.

A. Advantages

1) Cloud Infrastructure: GEE is mainly a free cloud-based service without having to download and manage data locally [35]. It is built upon the Google cloud computing infrastructure and computations are automatically handled by Google itself. All operations are automatically performed in bulk and parallel on the Google CPUs and GPUs [6]. The complexities of parallel computing are hidden due to this automation in processes [17].

Since GEE was mainly created and optimized for geospatial data analysis, it can process petabyte of RS data both in large geographical scales and in long temporal coverages [17]. Thus, it is a great tool for analyzing regional, national, continental, and global-scale applications.

Besides various datasets, which are already available within GEE, researchers can easily upload and share their own datasets as well as their scripts and models through URLs [9]. Other maps and products are generated on-the-fly [28], [29], once any user wants to run the code [36], [37]. Additionally, there is no need to install third-party software packages, such as ENVI and ERDAS, because almost all of the required tools are already available on GEE [38].

GEE stores and analyzes RS imagery based on a pyramiding and tiling concept [39]. Every image ingested into GEE has its pyramid at different pixel resolutions [6]. Furthermore, every tool used in GEE processes images on 256×256 tiles. Thus, different scales of the pyramid are used at various zoom levels. This enables GEE to visualize large areas of processed imagery quickly and efficiently.

Fast filtering and sorting capabilities are provided within GEE, inherited from Google. This enables users to select their desired data out of millions of images based on various spatial and temporal specifications [40].

2) API: GEE is combined with a powerful web-based programming interface. Users can easily access archived RS data through the JavaScript and Python API. The straightforward concept of using both APIs allows users to focus on the logic of data selection and programmable workflow. Only a log-in is required to access all GEE power. An online code editor is also available to write scripts, debug them, and see the results just after compilation.

Both the JavaScript and Python APIs provide access to the same set of EE objects and methods, except for a few methods which are capitalized differently (e.g., .and() versus .And()) [41], [42].

Most of the libraries in GEE are similar to existing open source components, such as OpenCV, and GDAL. Therefore, there is a minimum requirement to learn new concepts.

The Python API provides a programmatic and flexible interface to EE [41], [43]. It allows for automating batch

processing tasks, piping EE processed data to Python packages for postprocessing and leveraging the power of the command line. Additionally, the Jupyter notebook interface of the Google Colaboratory platform delivers a highly interactive and collaborative experience and is without the burden of local system setup and management as a hosted service. In summary, the EE code editor has a high ease of setup and use, while the Python API is more flexible. Combining GEE and Python APIs inside a Jupyter notebook provides the advantage of both to users.

In order to compare JavaScript with Python based on [43], it can be argued that JavaScript is easy to get started and share scripts, while it cannot share code between scripts. However, Python is easy to share code between scripts and is easier to be transformed into a web application. Moreover, Python has many plotting options, which requires several assembly and maintenance. Finally, the code editor enables the user to store, share, and control their codes in a behind-the-scene git environment.

3) Datasets: As discussed in Section III, GEE contains a large catalog of RS, geophysical, and meteorological datasets. It contains most of the important and temporal datasets in RS, including Landsat, MODIS, and Sentinel. Furthermore, the combination of different sources of imagery improves the temporal density of datasets and can help fusion algorithms to have more power. Moreover, several NRT datasets are uploaded to GEE in a daily manner. If a dataset is not in the GEE Data Catalog, it can also be uploaded to the servers. Datasets are also downloadable to continue from a desktop workstation at any point of the workflow.

GEE stores datasets in their original projection with all original data and metadata. Resolutions are managed directly by the platform. Data are stored in its original resolution, but a pyramid of images is also constructed and stored beside every image which is used in different zoom levels for the sake of efficiency. As mentioned, users can also easily search for their desired data using the tags provided within data categorization, which is very well handled in GEE.

Several preprocessing steps have been already applied to the datasets and, thus, users can use corrected data besides raw data. For instance, the orthorectified, atmospherically corrected, and Calibrated Top of Atmosphere Landsat data are easily accessible apart from the raw data [44], [45]. Analysis-ready SAR datasets on GEE represent a significant step forward because SAR preprocessing is relatively complex (especially for regular users). For example, GEE hosts Sentinel-1 GRD data preprocessed with ESA's SNAP software [46].

GEE makes many derivative products available. Multiple popular spectral indices (e.g., NDVI) are already calculated. Since storage is more expensive than computation, most of these derivative products are computed on-the-fly upon users' request.

4) Functions: As discussed in Section IV, a large set of functions and algorithms are available within GEE library for analyzing various datasets. All algorithms are parallel in nature and can automatically handle data management over servers.

Machine learning, image processing, vector processing, geometrical analysis, different visualizations, and multiple specialized algorithms are gathered into the GEE platform and enable users to implement their idea. The GEE functions usually satisfy the needs of a typical scientific project. Additionally, users can always implement their own algorithms outside GEE and return the result for postprocessing. For instance, TensorFlow is a better option in the deep learning section, for which more complex models, larger training datasets, more input properties, or longer training times are required [47], [48]. TensorFlow models are developed, trained, and deployed outside EE [49]. For easier interoperability, the EE API provides methods to import/export data in TFRecord format [47]. This facilitates generating training and evaluation datasets in EE and exporting them to a format where they can be ingested to a TensorFlow model.

A complete API reference and tutorial with runnable code examples are available for beginner to advanced users (e.g., [47]). The tutorials are detailed and cross referenced to each other to guide users through different applications and important notes. Outputs of these algorithms can be directly embedded in different applications.

B. Limitations

GEE limitations are relatively minor, but it is essential to be familiar with the constraints. Several main limitations of GEE are discussed in the following.

1) Although data is kept as private in the user's account, it is still stored in the servers of a private company, which is not acceptable for many governmental agencies and private companies [50].
2) GEE-based image analysis is restricted to existing tools within the GEE API. For example, several standard image preprocessing methods (e.g., atmospheric correction techniques) are currently not implemented in GEE. Moreover, developing new tools is not trivial and requires knowledge about all GEE algorithms and their functionality along with performance considerations about cloud-based computing on Google servers.
3) GEE is limited to selected data mining models for classification and regression. There are only a few classification and regression algorithms, such as CART, RF, and SVM.
4) Image classification as one of the important applications of RS can be considerably improved by object-based image analysis. However, currently, there is not an efficient and accurate segmentation algorithm within GEE [1].
5) One of the main approaches to improve classification accuracy is increasing the number of training samples or input features. However, users are limited to employ only a certain amount of samples or a limited number of features within classification methods [1], [16].
6) Complex machine/deep learning algorithms which require large training datasets or longer training times are not performed in GEE due to computational restrictions. Thus, users need to implement these algorithms outside of this environment [48].

TABLE II
TOP 10 JOURNALS PUBLISHING GEE-RELATED ARTICLES ALONG WITH THE NUMBER OF PUBLICATIONS PER JOURNAL

Journal	# Publications
Remote Sensing	126
Remote Sensing of Environment	61
ISPRS Journal of Photogrammetry and Remote Sensing	14
International Journal of Applied Earth Observation and Geoinformation	12
Forests	7
IEEE Journal of Selected Topics in Applied Earth Observations and Remote Sensing	7
Plos One	6
Science of The Total Environment	6
Computers and Geosciences	5
International Journal of Remote Sensing	5

TABLE III
GEE STUDIES PRESENTED AT THE TOP EIGHT CONFERENCES ALONG WITH THE NUMBER OF PRESENTED ARTICLES

Conference	#Publications
International Archives of The Photogrammetry Remote Sensing and Spatial Information Sciences ISPRS Archives	32
International Geoscience and Remote Sensing Symposium IGARSS	18
Proceedings of SPIE The International Society for Optical Engineering	8
40th Asian Conference on Remote Sensing Acrs 2019, Progress of Remote Sensing Technology for Smart Future	6
Proceedings 39th Asian Conference on Remote Sensing Remote Sensing Enabling Prosperity Acrs 2018	5
2019 10th International Workshop on The Analysis of Multitemporal Remote Sensing Images Multitemp 2019	4
38th Asian Conference on Remote Sensing Space Applications Touching Human Lives Acrs 2017	4
2019 8th International Conference on Agro Geoinformatics Agro Geoinformatics 2019	4

7) When trying to download processed data in the middle of the workflow for further analysis in a third-party software environment, users face a time-consuming process due to huge map size and internet speed limitations.
8) Complex SAR phase data are not stored in GEE because they are not compatible with the tiling concept of the infrastructure [51]. This limits the Polarimetric SAR and Interferometric SAR applications, which relies on the phase information.

VI. GEE PATTERN OF PUBLICATIONS

In this study, 450 journal papers, published between January 2010 and May 2020, were assessed to depict the pattern of GEE publications. Several investigations, including keyword analysis, annual publication numbers, and geographical distribution are provided in the following sections. Additionally, the top journals and conferences, which have published GEE papers are discussed in Section VI-E.

A. Analysis Method

A meta-analysis was performed in the Elsevier's Scopus (the largest abstract and citation database of peer-reviewed literature covering over 5000 publishers) and Web of Science (formerly known as ISI Thomson) to provide a comprehensive literature trend conducted using GEE. It is worth noting that conference articles and presentations were also reviewed during the course of this study; however, they were not considered in this study because most of them had a relatively lower academic level or had later been converted to journal papers. Only the top conferences, where GEE studies were presented, were provided in Table III. The *Google Earth Engine* and *GEE* search queries were performed in the journal articles' titles, abstracts, and keywords from January 2010 to mid-May 2020. The EndNote software was then used to remove the duplicate articles, which resulted in 462 peer-reviewed journal articles. Subsequently, 12 papers, which discussed unrelated topics (e.g., using GEE for gaming development and analyzing the computational performance of GEE) were discarded. Finally, 450 journal articles were selected for further analyses.

B. Keyword Analysis

Fig. 4 illustrates a word cloud visualization based on the keywords in these GEE studies. The more frequent the term appears within the keyword analysis, the larger the word depicts in the figure. As clear, *Google Earth Engine, Landsat*, *Remote Sensing*, *Sentinel-2*, *Random Forest*, *Cloud Computing, NDVI, Machine Learning,* and *Land Cover* were the mostly used keywords, respectively. For example, *Google Earth Engine* keyword was utilized in 278 papers. The name of different satellites and machine learning algorithms are also widely used in GEE publications. *Landsat*, *Sentinel-2*, *MODIS, Landsat-8,* and *Sentinel-1* are the satellites and *Random Forest* is the classification method, which are frequently utilized in the keyword lists of GEE journal papers. It was also observed that *NDVI*, *land*

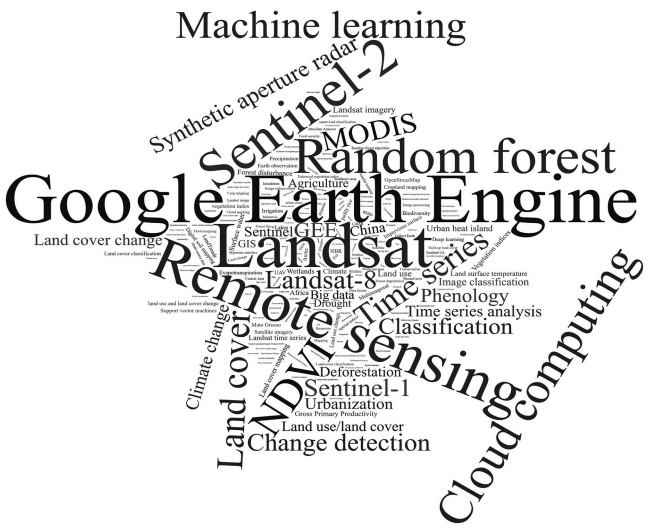

Fig. 4. Word cloud of the keywords from the GEE journal articles.

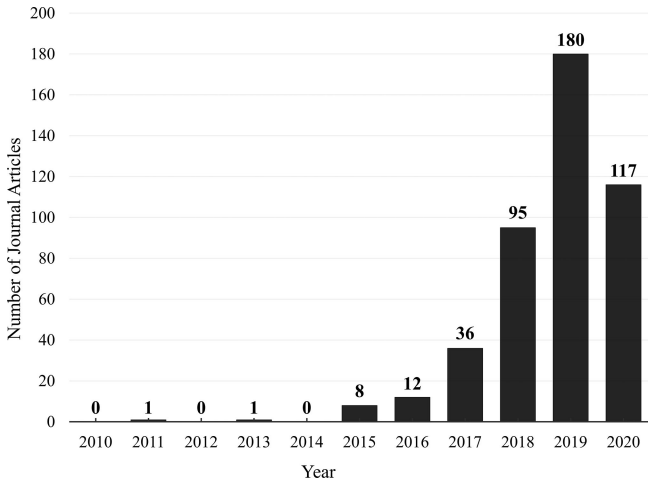

Fig. 5. Number of journal articles, which utilized GEE.

cover, *classification*, and *Urbanization* were among the most used keywords, indicating the popularity of LCLU classification applications. Additionally, the *Time Series*, *Change Detection*, *Climate Change*, *Land Cover Change*, and *Time Series Analysis* keywords were frequently utilized in the GEE publications, indicating the importance of the archived open-access remote sensing datasets in change detection studies. Furthermore, multiple journal publications used *China, United States,* and *Africa* in the keywords, demonstrating the leadership of the corresponding countries in utilizing GEE in their studies.

C. Annual Publication Numbers

The statistical analysis of the number of publications related to GEE is provided in Fig. 5. The first peer-reviewed journal paper was published in 2011 by Keller *et al.* [52] in *PFG - Journal of Photogrammetry, Remote Sensing and Geoinformation Science*. This study investigated the automated generation and presentation of historical 4-D city models. As clear from Fig. 5, a substantial increase in the number of GEE publications was observed from 2017, when Gorelick *et al.* [6] (GEE developers) discussed a comprehensive utility of this cloud computing platform, particularly for RS applications. Additionally, it was observed that the increasing trend in the number of GEE publications is getting more substantial. For instance, 35 journal articles were published within the last 1.5 months (April 1–May 15, 2020).

D. Geographical Distribution

The study areas of the peer-reviewed GEE journal papers were investigated to provide a picture of the geographic distribution of GEE studies. Fig. 6 illustrates the geographical distribution of GEE studies after removing ten papers, which did not belong to any study areas (e.g., literature review papers and papers related to the theoretical aspects and development of the GEE platform). Additionally, 35 studies which were conducted over the continental scales (7 and 1 papers covered the entire Africa and Europe, respectively) and global scales (27 papers covered the entire world) were not considered in a country-based enumeration. Furthermore, if a study was conducted over several countries, all of them were counted separately. Moreover, studies with sub-country scales (e.g., small study site, city, or province) were considered in the number of publications for the corresponding countries. Finally, it was observed that GEE studies were conducted over 138 countries. The highest number of GEE publications have been conducted over the United States (97 articles), China (96 articles), Brazil (29 articles), Canada (25 articles), and India (25 articles), followed by Australia (19 articles), and Indonesia (15 articles), respectively. On the continental scale, 37.5%, 24%, 18.5%, 9%,7.5%, 3.5%, and 0% of studies were conducted over Asia, North America, Africa, Europe, South America, Australia, and Antarctica, respectively. 38% of studies conducted over Asia were related to China.

E. Journals and Conferences

Table II provides the top journals, in which GEE studies have been published. 450 journal papers have been published in 150 journals, 95 of which have published only one GEE paper. Based on the results, the *Remote Sensing*, *Remote Sensing of Environment*, *ISPRS Journal of Photogrammetry and Remote Sensing*, and *International Journal of Applied Earth Observation and Geoinformation* were the top four journals, which published 126, 61, 14, and 12 papers, respectively.

Table III provides the name of several conferences, in which GEE studies have been most frequently presented. GEE studies are among the most presented research topics in the prominent international RS conferences, such as the *International Archives of the Photogrammetry Remote Sensing and Spatial Information Sciences ISPRS Archive*, the *International Geoscience and Remote Sensing Symposium IGARSS*, and the *Proceedings of SPIE The International Society for Optical Engineering*.

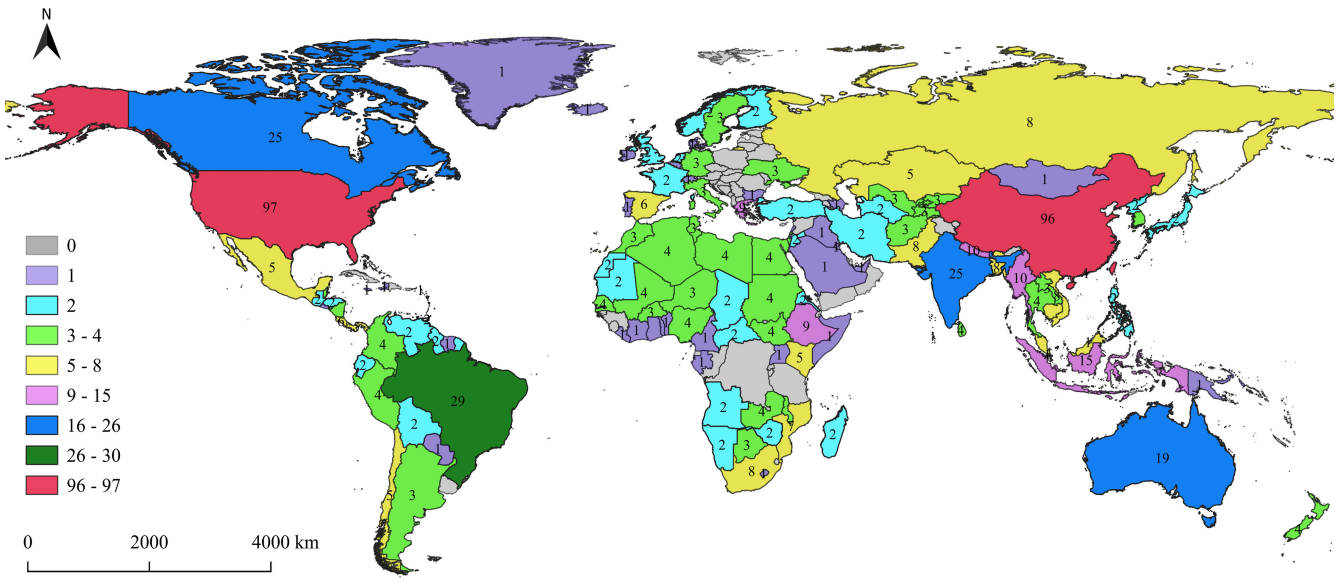

Fig. 6. Number of GEE studies conducted over each country.

VII. GEE Applications

The 450 selected GEE journal articles were studied to decide about the main disciplines. It is worth noting that seven papers which were review articles were initially removed from the analysis. Consequently, all the 443 journal papers were divided into 10 categories as illustrated in Fig. 7 along with several keywords describing each category. The articles which include more than one application were considered in the most relevant category by an in-depth review of the paper. It is worth noting that although only the journal articles were investigated to adopt the main disciplines, it was observed that other sorts of publications (e.g., conference papers) correspond well with the application types considered in this study.

Fig. 8 illustrates the number of journal articles related to each application provided in Fig. 7. The highest number of contributions were in the *Vegetation* category with 90 papers followed by 77 papers in *Agriculture*, 68 papers in *Hydrology*, 53 papers in *Land cover*, 40 papers in *Urban*, 40 papers in *Natural disaster*, 31 papers in *Atmosphere and climate*, 17 papers in *Image processing*, and 14 papers in *Pedosphere*. Moreover, 13 papers, which were not related to any of the 10 application types or their numbers and not enough to be assigned to a new category were considered in the *Others* category.

In the following sections, more information about each of the GEE applications along with several case studies are discussed.

A. Vegetation

Vegetation (e.g. forest, grassland, rangeland, and shrub) can be considered as one of the most vital components of the Earth's biosphere because it serves critical functions to both humans and the environment [53]. Vegetation is also important in many biochemical cycles that are directly or indirectly interacting with water, soil, and air [54]. Such cycles are important for global vegetation pattern and climate studies and, thus, vegetation is also important for biodiversity conservation and climate change mitigation [55]. Moreover, vegetations are the primary source of converting dioxide carbon to oxygen, enabling aerobic metabolism on the globe [56]. Considering the important services of vegetation, it is highly required to monitor the current state and dynamics of various vegetation types. GEE leverages cloud computing services for long-term monitoring of vegetation covers. Furthermore, the publicly available RS data within GEE enable researchers to employ this platform for vegetation monitoring at various spatial scales. In particular, the existence of several vegetation indices in GEE allows conducting vegetation studies in efficient and quick manners. GEE has been widely used for vegetation mapping [57], [58], vegetation dynamics monitoring [59], [60], deforestation [61], [62], vegetation and forest expansion [63], [64], forest health monitoring [65], [66], forest mapping [67], [68], pasture monitoring [49], [69], and rangeland assessment [70], [71]. For instance, the full archive of the Landsat imagery was processed within GEE to map the vegetation dynamics from 1988 to 2017 in Queensland, Australia [59]. Field observations were utilized to evaluate the performance of the proposed algorithm and an overall accuracy of 82.6% was reported. Finally, the suitability of GEE for large-scale and long-term vegetation monitoring was reported along with an approximately 20% decrease in the vegetation cover in this study area. The authors emphasized the high computational efficiency of GEE compared to when they did the same analysis using traditional methods. In another study, an algorithm was developed within GEE by employing spectral mixture analysis to detect degradation and deforestation in the Brazilian state of Rondônia [62]. To this end, Landsat archived images from 1990 to 2013 were used. All the required processing steps were performed within GEE to produce annual

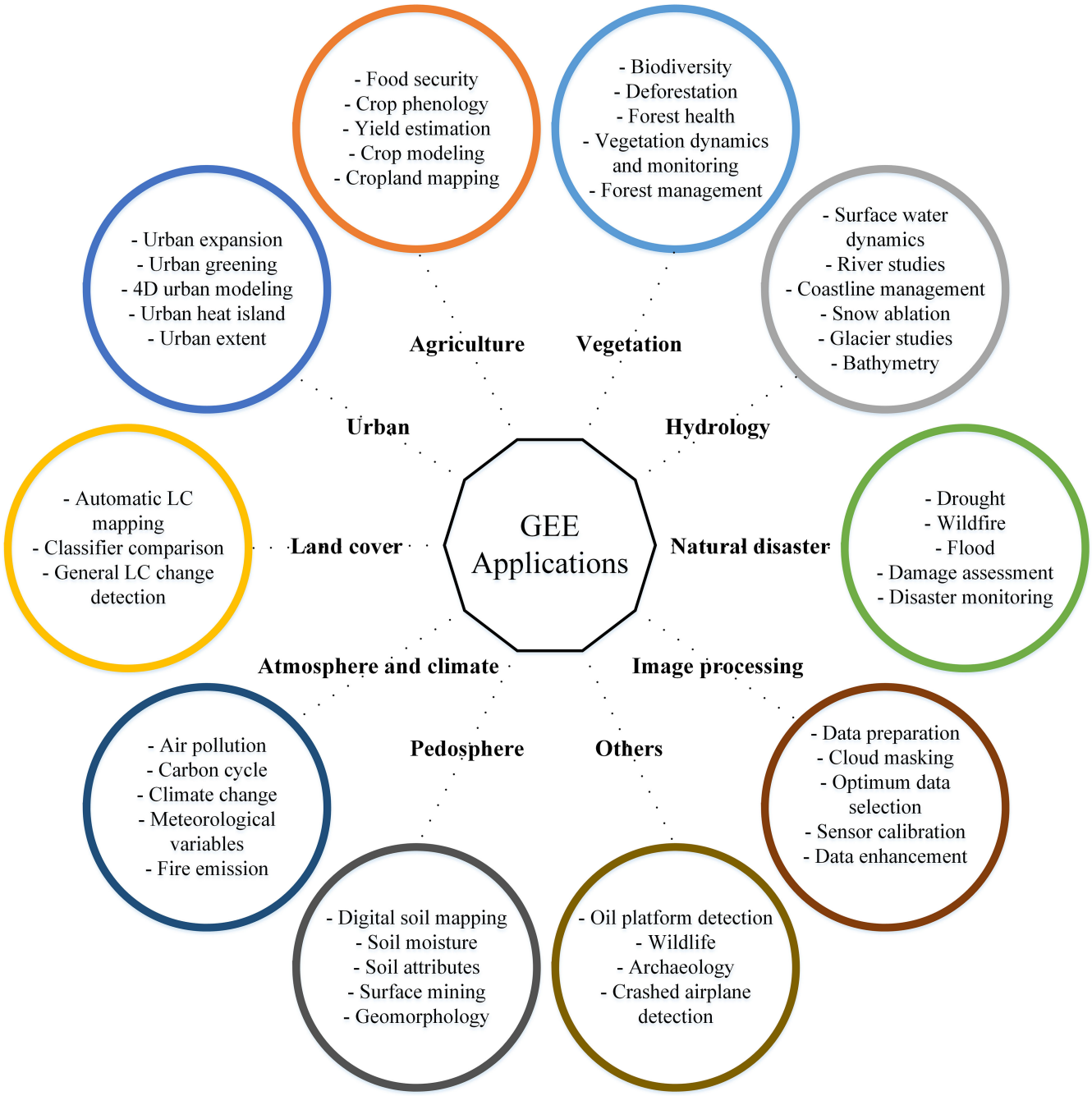

Fig. 7. GEE applications (LC: Land Cover).

forest disturbances maps. Landsat data were transformed into spectral endmember fraction and were applied to calculate the Normalized Degradation Fraction Index. The presented method obtained producer accuracies of 68.1% and 85.3% for degradation and deforestation maps, respectively.

B. Agriculture

Mapping and monitoring croplands and plantations are essential for food security. Food security could be stated as one of the most significant issues in the current era and, thus, the Food and Agriculture Organization (FAO) has set its goal to achieve food security around the globe [72], [73]. Agricultural products not only play a vital role in human life, but also are critical from economic aspects. Therefore, agriculture can be considered as a source of livelihood and a contributor to national revenue [74]. Moreover, monitoring agricultural products is required for policy-makers and governments to ensure the path to economic growth and self-sufficiency of the country [72]. RS datasets allow frequent and cost-effective monitoring of croplands and plantations. GEE hosted extensive publicly available RS datasets that can be effectively utilized for productivity, quality,

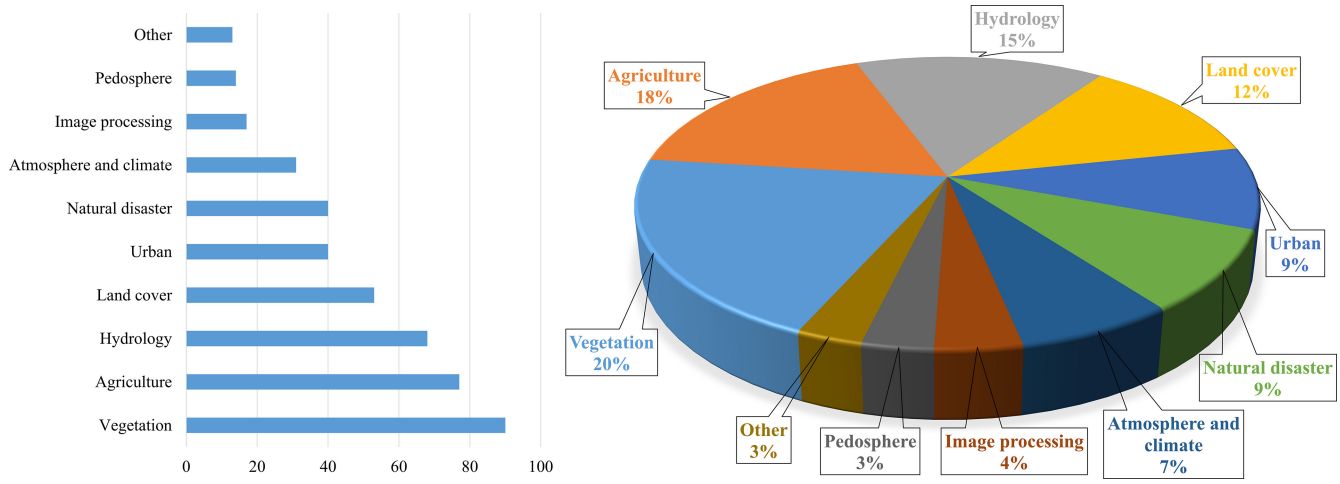

Fig. 8. Number and percentage of journal papers related to GEE applications, published in each discipline provided in Fig. 7.

profitability, and sustainability studies of agriculture production. Researchers have applied GEE to plantation mapping and monitoring [75], [76], phenology-based classification [77], [78], cropland mapping [79], [80], crop condition monitoring [81], [82], crop yield estimation [83], [84], irrigation mapping [85], [86], and other agricultural studies [87], [88]. For example, seasonal median composites of Sentinel-1 and Sentinel-2 were calculated in GEE to predict the Maize yield in Kenya and Tanzania [83]. The use of RF resulted in the production of Maize/none Maize maps in Kenya and Tanzania with 63% and 79% overall accuracies, respectively. Finally, satellite observations along with gridded soil datasets were ingested into a scalable harmonic regression to estimate Maize yield. Moreover, multitemporal Landsat-8, Landsat-7, and Sentinel-2 imagery were employed to calculate composite NDVI images for winter cropland mapping in an area of over 200 000 km^2 [77]. Then, the multitemporal NDVI curve was inserted into a CART algorithm to produce a phenology-based map of winter cropland with an overall accuracy of 96.22%. The authors reported that lacking remote sensing images with high temporal frequency in GEE was one of the limitations of their work and, thus, suggested to use Chinese GaoFen satellite data with four days revisit time for the future cropland classifications.

C. Hydrology

Water is an essential element for life whether in liquid form (e.g., lake, reservoir, and river) or solid forms (e.g., snow, ice, and glaciers) in the cryosphere and, thus, obtaining reliable information about water resources is a high necessity. In addition, monitoring inland, coastal, and arctic water resources are beneficial in climate change studies [89]. Moreover, investigating the size and behavior of glaciers along with the amount of snow ablation could render supporting information about the Cryosphere–Atmosphere interactions and climate change [90], [91]. Furthermore, drought and flood disasters are relatively associated with the dynamics of water resources [92]. Therefore, persistent and precise monitoring of all types of water resources is a vital need. Publicly available datasets within GEE along with its high computing performance allow for accurate monitoring of water resources with adequate temporal and spatial resolutions. Consequently, GEE was efficiently employed for surface water dynamics monitoring [93], [94], bathymetry [20], [95], shoreline and coastal studies [96], [97], lake and reservoir mapping and monitoring [98], [99], glacier studies [90], [100], snow ablation and snow mapping [92], [101], suspended sediments and river studies [102], [103], and water health assessment [104], [105]. For instance, Nguyen *et al.* [93] introduced a fully automatic method for water extraction in New Zealand. The GEE and Landsat-8 images between 2014 and 2018 were employed to map lakes and reservoirs using an Automatic Water Extraction Index with an overall accuracy of 85%. In a different study, GEE was used to combine MODIS fractional snow cover with Sentinel-1 wet snow mask data to develop an algorithm to produce a monthly wet-dry snow map [92]. In this study, 2.5 years were studied in the Indian Himalayan region covering around 55 000 km^2. It is worth noting that the underestimation of the wet snow area was corrected by DEM. In another study, blue and green bands of Sentinel-2 were processed to develop an empirical model for satellite-derived bathymetry maps [20]. In this regard, cloud masking, sun glint correction, radiometric calibration, and normalization were performed within GEE in three sites of the Aegean Sea in the Eastern Mediterranean. Finally, based on 9818 reference points, the proposed approach achieved R^2 and RMSE of 0.9 and 1.67 m, respectively. The authors argued that GEE *time-out* error was the main limitation in their work, because their empirical method required estimation of the regression between the image composite values and water depth over large region and a long period of time.

D. Urban

Urban areas are regions with concentrated people and human infrastructure and usually expand through the time for better livelihood. These regions have become the central point of economic, social, cultural, and recreational activities, as well as

resource consumption [106], [107]. Therefore, urban areas could be considered as the primary source of human interaction with the surrounding environment. The environment and the urban areas affect each other mutually since the environmental changes could influence human life. On the other hand, unrestricted urban growth causes severe damage to natural resources and can negatively alter the atmosphere and climate [108], [109]. Conducting urban studies are essential to support sustainable development. In this regard, RS datasets enable the quantification and profound analysis of urban dynamics that are fundamental for devising suitable approaches for urban development and urban planning [110]. GEE promotes long-term monitoring of urban conditions to effectively study the urban environment from different aspects. Urban expansion and extent mapping [18], [111], urban morphology and local climate zone monitoring [112], [113], urban 4-D modeling [52], urban green space classification [114], [115], urban temperature and urban heat island identification [17], [110] are some of the main urban studies conducted within GEE. For instance, Ravanelli *et al.* [17] studied the long-term monitoring of Surface Urban Heat Island (SUHI) and its relation to urban land cover changes over six metropolitan areas of the United States. More than 6000 Landsat images were interpreted between 1992 and 2011 by Detrended Rate Matrix analysis to illustrate the land cover change versus SUHI. It was reported that GEE was the best solution for their applications in terms of efficiency in time, cost, and computation. The results revealed a definite increase of SUHI due to urban growth. Moreover, Gong *et al*. [18] investigated the urban expansion dynamics by producing annual global artificial impervious surfaces that are predominate indicators of human settlement. To this end, the full archives of Landsat satellite data between 1985 and 2018 were processed within GEE. Sentinel-1 SAR data and nighttime images were also used to improve the final results in arid areas. The implementation of the Exclusion–Inclusion algorithm combined with the temporal consistency check within GEE yielded the overall accuracy of over 90% in mapping annual global impervious surfaces.

E. Land Cover

The dominant land cover types of a region determine the terrestrial surface characteristics of the corresponding area. Vegetation, water, and soil are the main land cover types spread across the globe. These land cover types form environmental conditions for the habitat of various flora and fauna [116], [117]. Furthermore, the distribution of land covers defines the physical interaction between Earth's surface and the surrounding environment. Recognizing the significant impacts of land covers on the environment and investigating the current condition along with monitoring long-term dynamics of land covers are essential for sustainable development, climate change modeling, biodiversity studies, and natural resource monitoring [118], [119]. GEE hosted enormous publicly RS datasets in various spectral and spatial resolutions to conduct land cover mapping [14], [120], land cover dynamics monitoring [121], [122], coastal mapping [123], [124], and wetland classification [125]. For instance, an automatic land cover mapping was developed within GEE through the integration of Landsat imagery and RF algorithm over the north of China [14]. The reference samples were collected by rules of pixel and spectral filtering from MODIS land cover products with the International Geosphere-Biosphere Program theme in ten classes. Two types of monthly and percentile features were utilized separately, and the best result was obtained through the usage of monthly features by achieving over 80% accuracy. In another study, GEE was used to produce a sharpened land cover map over Mato Grosso, Brazil [15]. Their proposed algorithm (BULC-U) fused the 300 m the *GlobeCover* product with Landsat imagery to produce a 30 m land cover map. In this regard, Landsat images were segmented and then the ISODATA algorithm was applied to generate an unsupervised map in 20 clusters. Finally, the unsupervised classification result was fused to the *GlobeCover* product. More recently, Ghorbanian *et al.* [126] produced an improved version of the land cover map of Iran using Sentinel-1/2 imagery within GEE. They also proposed an automatic workflow to update this map every year without the need to collect additional *in situ* data using migrated samples.

F. Natural Disaster

Extreme and unexpected phenomena caused by the natural process of the Earth are called natural disasters. These events bring destruction to the surrounding environment and human life [127]. Profound research should be carried out to investigate the characteristics and behavior of these phenomena and, consequently, to reduce the amount of damage. The importance of geospatial data for monitoring and damage assessment of natural disasters is undeniable [128]. Long-term and NRT publicly available RS datasets within GEE along with its high-performance computing promote this cloud-based platform for monitoring, forecasting, prevention, vulnerability, and resilience studies of natural disasters. In particular, GEE was utilized for drought monitoring [129], [130], flood mapping and flood risk assessment [131], [132], wildfire severity mapping [133], [134], landslides analyses [135], hurricane studies [136], and tsunami studies [137]. For instance, MODIS and meteorological datasets were employed within GEE to study the temporal and spatial variations of drought events in Potohar Plateau of Punjab, Pakistan between 2000 and 2015 [129]. In this regard, multiple features of standard precipitation index, standard precipitation-evapotranspiration index, vegetation condition index, precipitation condition index, soil moisture condition index, and temperature condition index were utilized for drought monitoring. In addition, 44 Sentinel-1 GRD dual-polarized data were employed within GEE to develop an operational methodology for rapid flood inundation mapping in Bangladesh [131]. Moreover, a potential flood damage map was generated to support efficient decision making. The proposed method obtained 96.44% overall accuracy by incorporating 4500 reference samples. Finally, a preflood Landsat-8 image was used to generate a land cover map for further estimation of flood damages to cropland and rural settlements. It was reported that the developed algorithm within GEE could be effectively used for monitoring land covers in

a cost-efficient approach because open-access Landsat datasets are regularly inserted into GEE. In a different study, very high-resolution oblique images were processed within GEE to detect irregularity in façade and rooftop areas caused by hurricane events [136]. First, a vertical building map was produced from a temporal analysis of predisaster images through an edge-based/knowledge-based approach. Then, pre- and postdisaster images were fused in the data level followed by spectral-only and geospectral classifiers through the RF algorithm. The results obtained a significant reduction in false-positive error.

G. Atmosphere and Climate

As a principal component of the natural process of the Earth system, land interacts with the atmosphere through biophysical and biochemical processes mutually [138]. Constant population growth and human activities result in significant changes in the atmospheric constituents [139]. Climate change and air pollution are two decisive consequences of these disturbances that directly impact the surrounding environment and human health [140], [141]. Therefore, it is essential to monitor and control air quality and climate conditions to avoid severe outcomes. The availability of climate products accompanied by surface products within GEE, make this platform a great tool for climate studies and air quality monitoring. These advantages create a rising interest in the research community to use GEE for air pollution analyses [142], [143], climate change and monitoring [144], [145], biophysical variable studies [21], [146], evapotranspiration estimation [147], and precipitation mapping [148]. For instance, GEE was employed to map exposed mine waste areas to estimate the corresponding emission of particulate matter to the atmosphere [142]. Four benchmark years of 1990, 2000, 2010, and 2018 as a part of Canada's Air Pollutant Emission Inventory were studied. Landsat-5, Landsat-8, Sentinel-1, and Sentinel-2 satellite data were used to map exposed mine through an RF algorithm. Finally, the authors reported that GEE was an invaluable platform for monitoring long-term emission from exposed mine waste. Furthermore, GEE was used along with version 1 Tropical Rainfall Measuring Mission (TRMM) precipitation products to study the spatial and temporal patterns of precipitation in the Zambezi River basin [148]. To this end, TRMM data from 1998 to 2017 were processed in GEE to investigate the precipitation trends and magnitudes by Kendall's correlation and Sen's slope reducer respectively. A "dry gets dryer, wet gets wetter" pattern was observed and reported in the study region.

H. Image Processing

In the current era, almost all EO platforms are equipped by digital sensors and, thus, terabytes of data are generated and stored in digital formats every day. As discussed, GEE hosts an immense number of digital images. The RS images are extensively utilized in various applications and for different purposes. Therefore, it is highly required to develop and enhance digital image processing algorithms to efficiently exploit the potential of digital images. Moreover, since the quality of every input data directly affects the final accuracy of studies, image processing must be considered a necessity. Precision, level of automation, reliability, computational complexity, and time-consumption are the most critical criteria in developing image processing algorithms [149], [150]. Therefore, to ensure high-quality results, it is inevitable to develop and enhance the existing image processing algorithms within GEE protocols. In this regard, researchers have employed GEE to develop various efficient and useful image processing algorithms, such as cloud masking [12], [149], data selection and enhancement [13], [150], image-based sensor calibration [151], [152], and training sample migration [153]. For instance, Kong *et al*. [150] introduced weighted Whittaker with a dynamic parameter (wWHd) denoising method within GEE to reconstruct the vegetation phenology based on 500 m MODIS EVI products. A large number of reference samples were used to compare the proposed method with four well-known denoising methods. The results, in terms of RMSE, roughness, and computational efficiency revealed the superiority of the proposed method. Furthermore, Li *et al*. [13] developed an algorithm to improve GEE's processing to efficiently acquire large-scale cloud-free Landsat images to support further applications. This method comprises cloud and shadow masking, snow/ice masking, and low-quality pixels removal by incorporating the quality band. Therefore, this method can efficiently prepare high-quality data for each region of interest. It was discussed that their algorithm was developed within GEE, and the open-access codes within this platform provided a simple framework with a flexible user-friendly interface. Finally, Kakooei *et al.* [154] proposed a global Sentinel-1 foreshortening mask to improve the reliability of SAR-based analysis.

I. Pedosphere

The Pedosphere is the outermost layer of Earth which dynamically interacts with the Biosphere and atmosphere [155]. Monitoring and studying the Pedosphere and the corresponding categories (e.g., soil, geology, and geomorphology) are prerequisites for sustainable development, especially in the climate modeling context [156]. Soil is the most significant component of the Pedosphere that has straight impacts on the surrounding environment and, thus, essential for biodiversity conservation and climate regulations [157]–[160]. The availability of RS datasets in GEE makes it an appealing platform for the Pedosphere studies at diverse scales. GEE was utilized for digital soil mapping [50], [161], geology and mining [162], [163], geomorphology studies [164], soil topography mapping [165], soil moisture derivation [166], and soil carbon and salinity estimation [167], [168]. For example, Ivushkin *et al*. [168] applied Landsat-5 and Landsat-8 datasets within GEE to produce a global soil salinity map based on the thermal anomaly. They incorporated 15 188 reference points from ISRIC-world soil information. Seven soil salinity indicators of sand content, silt content, clay content, PH, bulk density, organic carbon content, and cation exchange capacity with thermal anomaly were fed to the RF algorithm. The final soil salinity map obtained overall accuracies of 67%–70% for

six different times. Moreover, GEE capabilities and Landsat imagery were combined to automatically delineate the annual extent of surface coal mining in Central Appalachia between 1985 and 2015 [162]. To this end, the urban areas were masked using publicly available datasets and the mining zones were identified by low values in NDVI images. The proposed algorithm achieved Kappa coefficients varying from 0.62 to 0.93 for different years.

J. Others

Other than previously mentioned applications, there are multiple articles related to other applications of GEE, which were conducted with lower frequency. Therefore, their number was not enough to have a separate category and, thus, were assigned to the *Others* applications category. These studies are mainly related to archaeology [169]–[171], 3-D printing [172], wildlife [173], [174], oil platform detection [175], and crashed airplane detection [176]. For example, 300 Landsat-8 images between 2013 and 2018 were processed in GEE to detect possible crashed airplane in the Cambodian jungle [176]. NDVI, albedo, thermal bands, spectral information, and panchromatic features were utilized in this study. Moreover, Sentinel-1 SAR data were used to automatically identify and delineate offshore oil platforms [175]. The proposed method was evaluated by 1577 reference samples and obtained an overall accuracy of 96.09% over the Gulf of Mexico. Furthermore, GEE was reported as a suitable platform to process high-resolution drone imagery for pottery shreds identification [169]. In this regard, texture and gradient features from RGB drone imagery were calculated within GEE and were ingested into the RF classifier. The developed algorithm was able to identify pottery shreds with 32.9% and 76.8% accuracies for two separate regions. Moreover, GEE was employed to process drone imagery to estimate the wildlife aggregation population [173]. To this end, the RF algorithm was applied to map targets of interest (bird nest) pursuit using a predictive model to estimate the population. The proposed approach obtained overall accuracies ranging from 86% to 96% over four different water bird colonies. Finally, a web-application called *TouchTerrian* was developed to simplify the 3-D terrain model printing [172]. After determining the region of interest, the corresponding DEM was obtained through GEE to be used for final 3-D printing. It was reported that users with any level of expertise could easily utilize their model within GEE with minimum computing resources requirements.

VIII. GEE Large-Scale Case Studies

As discussed, the enormous capabilities of GEE resolve the existing challenges of processing big data over large-scale areas. Therefore, GEE has been recognized as an efficient platform for regional to global LC mapping and monitoring over long periods of time. In this section, ten studies conducted over the globe, continents, and big countries (e.g., the United States, Canada, and China) are discussed in detail.

A. Globe

Long *et al.* [133] proposed an automatic method for producing a global annual burned area maps using all available Landsat images acquired between 2014 and 2015 within the GEE cloud computing platform. The map of the burn degree was first generated using the RF classifier. Then, several logical filters (e.g., NDVI, Normalized Burned Ratio (NBR), and temporal filters) were implemented to select candidate seeds of the burned area. Finally, the global annual burned area map of 2015 (GABAM 2015) was produced by employing an iterative seed-growing process. A strong correlation ($R^2 = 0.74$) was observed between the spatial distribution of the burned surfaces from the GABAM 2015 and the annual 250 m MODIS Vegetation Continuous Fields (VCF) Collection 5.1 (MOD44B) product.

Hansen *et al.* [8] analyzed forest cover changes at the global scale between 2000 and 2012 using Landsat time-series images within GEE. Based on the results, the authors reported the following:

1) the tropical domain had the highest forest cover change (loss and gain) with annual deforestation rate of approximately 2101 km^2/year;
2) most forests in the subtropical climate domain were considered as croplands, because the existence of long-lived natural forests in this domain was relatively rare;
3) the trend of change in temperate forests was almost constant and had a low ratio of loss compared to gain;
4) fire was the most important cause of deforestation in the boreal domain;
5) the speed of deforestation in Brazil was more than other countries.

In [177], a grid-based Mountain Green Cover Index (MGCI) was implemented to monitor mountain ecosystems at large scales. A novel frequency- and phenology-based technique was applied to generate the global green vegetation cover using all available Landsat-8 images within the GEE platform. Then, the real surface area generated from ASTER GDEM Version 2 was applied to calculate the MGCI model instead of the planimetric surface. The results showed that the generated data had a high correlation ($R^2 = 0.9548$) with FAO MGCI baseline data.

In [178], global surface water and its long-term changes were mapped over three decades of Landsat satellite images (three million images) within the GEE platform. The result of this global assessment demonstrated the following:

1) permanent water bodies disappeared by approximately 90 000 km^2 and new water bodies covering 184 000 km^2 formed between 1984 and 2015;
2) the permanent net water of all continental regions increased except for Oceania;
3) over 70% of global net permanent water loss occurred in the Middle East and Central Asia due to drought and human actions (e.g., river damming).

It is finally argued that the proposed strategy within GEE can be effectively used for water resources management.

Scherler *et al.* [90] proposed a novel automatic method to map supraglacial debris cover over the globe using multitemporal

optical satellite images within GEE. In this study, debris-covered ice surfaces were generated by thresholding of three indices, including red to Shortwave Infrared band ratio, the Normalized Difference Snow Index, and linear spectral unmixing-derived Fractional Debris Cover. These indices were generated based on Landsat-8 and Sentinel-2 optical satellite images in 19 glacier areas at the world-scale from 2013 to 2015. The results showed that 4.4% (about 26 000 km²) of all glacier areas is affected with debris. Furthermore, an inverse relationship between glacier size and percentage of debris was also reported, indicating continuous shrinking glaciers due to the debris effects.

B. Continent and Big Countries

Amani *et al.* [1] produced the first Canadian wetland inventory (CWI) map using Landsat-8 imagery and several advanced algorithms available within GEE. In this study, 30 000 scenes of Landsat-8 images were used along with machine learning algorithms in GEE. The RF algorithm was applied to classify wetlands over the entire Canada. The CWI map was based on five wetland classes, defined by the Canadian Wetland Classification System: bog, fen, marsh, swamp, and shallow water. The quantity and quality of the results showed that the generated CWI map had reasonable accuracy considering the challenges existing over this immense country (9.985 million km^2).

Li *et al.* [179] generated African LCLU map at a 10 m resolution within GEE using multisource RS datasets, including Sentinel-2, Landsat-8, Global Human Settlement Layer, Night Time Light data, Shuttle Radar Topography Mission (SRTM), and MODIS Land Surface Temperature images. The RF algorithm was applied to classify the area into five categories of urban, trees, low plants, bare soil, and water. The results showed that the LCLU map generated by this method had a better performance than that of the FROM-GLC10 [180] in detecting urban class and distinguishing trees from low plants in rural areas.

Beresford *et al.* [181] developed an NRT monitoring framework for conservation of the Key Biodiversity Areas (KBAs) in Africa using the GEE platform. In this study, simple repeatable techniques were proposed to detect changes in fire rate, tree loss, and nighttime lights between 1992 and 2013. The results showed that fire rate, nighttime lights, and rate of forest loss considerably increased in KBAs and ecoregions. Moreover, the authors argued that the method implemented within GEE has a high potential for monitoring changes over any geographic area and using different RS data types and could be effectively utilized by conservation end-users.

Teluguntla *et al.* [182] developed a precise Landsat-based cropland extent product over Australia and China using machine learning tools in GEE. In this study, cropland maps were produced by applying RF to Landsat-8 images. The RF classifier was trained and validated using ground truth data obtained from different resources, such as field surveys, very high spatial resolution (5 m) imagery, and several other auxiliary information. Based on their results, the total cropland areas of Australia and China were estimated as 35.1 and 165.2 million hectares, respectively.

Goldblatt *et al.* [183] used GEE for temporal analysis of large urban areas in India using multitemporal Landsat-7 and Landsat-8 images. In order to generate high-quality maps of built-up areas, the country was classified into the built-up and non-built-up regions using 21 030 training datasets and three types of supervised classification algorithms (i.e., SVM, CART, and RF). It was reported that the proposed GEE approach generated a high-quality map of built-up areas in India and can be potentially employed in other countries.

IX. Conclusion

The proliferation of big geo data and the recent advance in cloud computing and big data processing services are changing the future of RS. In this regard, GEE is effectively paving the road for researchers, scientists, and developers to be able to easily extract valuable information from big RS datasets without the burdens of traditional data analysis methods. The massive troves of RS datasets available with GEE (e.g., archived Landsat and Sentinel images) helps researchers to address global challenges and environmental issues, such as global warming, climate change, LCLU classification over large areas, and monitoring landscape over several decades. GEE also contains hundreds of prebuilt functions which can be easily understood and utilized by different users. Through a basic knowledge of JavaScript, users can also implement their own algorithms. These advantages make any user employ this cloud computing platform for various applications related to LCLU, agriculture, hydrology, natural disaster, etc. Besides all the advantages, it also has several limitations, such as limited storage of 250 GBs for each user and limited memory to train machine learning algorithms, which may push a new user backward. However, it is undeniable that GEE presents a novel way of processing geospatial data and resolves several big data challenges existed for RS researchers. Based on the GEE publication trends, it is also clear that this platform is becoming more popular not only among the RS researchers but also within any community interested in using EO datasets.

Authors' contribution

Meisam Amani designed and supervised the study, professionally optimized all sections, acquired funding, wrote the Abstract, Introduction, and Conclusion; Arsalan Ghorbanian wrote the "GEE Applications" section; Seyed Ali Ahmadi wrote the "GEE Advantages and Limitations" section; Mohammad Kakooei wrote the "GEE Datasets" and "GEE Functions" sections; Armin Moghimi wrote the "GEE Large-scale Case Studies" section; Seyed Mohammad Mirmazloumi gathered the required articles and wrote the "GEE Pattern of Publication" section; Sayyed Hamed Alizadeh Moghaddam wrote the "GEE Platform Overview" section; Sahel Mahdavi professionally optimized all sections; Masoud Ghahremanloo helped in initial literature review; Saeid Parsian helped in gathering the required articles; Qiusheng Wu and Brian Brisco professionally optimized all sections. Finally, all authors read and approved the final manuscript.

APPENDIX

TABLE IV
LIST OF AVAILABLE DATASETS WITHIN GEE

Type	Data	Resolution	Coverage	Temporal	Products
Landsat	Landsat-1 MS	60 m (NIR2- 30 m)	Sample Tiles	(1972-1978)	-
	Landsat-2 MS			(1975-1982)	-
	Landsat-3 MS			(1978-1983)	-
	Landsat-4 MS	30 m	Global	16 day (1982-1993)	Burn Area Index (BAI) Enhanced Vegetation Index (EVI) Normalized Difference Vegetation Index (NDVI) Normalized Burn Ratio Thermal (NBRT) Normalized Difference Snow Index (NDSI) Normalized Difference Water Index (NDWI)
	Landsat-5 MS			16 day (1984-2012)	
	Landsat-7 MS	30 m (Pan- 15 m)		16 day (1999-Present)	
	Landsat-8 MS			16 day (2013-Present)	
Sentinel	Sentinel-1 SAR	10 m	Global	6 day (2014-Present)	-
	Sentinel-2 MS	10/ 20 m		10 day (2015-Present)	-
	Sentinel-3 Ocean and Land Color Instrument	300 m		2 day (2016-Present)	-
	Sentinel-5P TROPOspheric Monitoring Instrument	0.01 arc		1 day (2018-Present)	UV Aerosol Index Cloud Carbon Monoxide Formaldehyde Nitrogen Dioxide Ozone Sulfur Dioxide Methane
Modis daily	MOD09GQ.006	250 m	Global	1 day (2000-Present)	Terra Surface Reflectance
	MCD43A4.006	500 m			MODIS Nadir BRDF-Adjusted Reflectance
	MCD43A3.006				MODIS Albedo Daily
	MCD43A2.006				MODIS BRDF-Albedo Quality
	MCD43A1.006				MODIS BRDF-Albedo Model Parameters
	MOD10A1.006				Terra Snow Cover
	MOD11A1.006	1 km			Terra Land Surface Temperature and Emissivity
	MOD09GA.006				Terra Surface Reflectance
	MODOCGA.006				Terra Ocean Reflectance
	MOD14A1.006				Terra Thermal Anomalies & Fire
MODIS	MOD09Q1.006	250 m	Global	8 day (2000-Present)	Terra Surface Reflectance
	MOD13Q1.006			16 day (2000-Present)	Terra Vegetation Indices
	MOD44W.006			Yearly (2000-Present)	Terra Land Water Mask
	MOD44B.006				Terra Vegetation Continuous Fields
	MCD15A3H.006	500 m		4 day (2002-Present)	MODIS Leaf Area Index
	MOD09A1.006			8 day (2000-Present)	Terra Surface Reflectance
	MOD17A2H.006				Terra Gross Primary Productivity
	MOD16A2.006			8 day (2001-Present)	Terra Net Evapotranspiration
	MOD13A1.006			16 day (2000-Present)	Terra Vegetation Indices
	MCD64A1.006			Monthly (2000-Present)	MODIS Burned Area
	MCD12Q1.006			Yearly (2001-Present)	MODIS Land Cover Type
	MOD17A3H.006			Yearly (2000-Present)	Terra Net Primary Production
	MOD11A2.006	1 km		8 day (2000-Present)	Terra Land Surface Temperature and Emissivity
	MOD14A2.006			8 day (2000-Present)	Terra Thermal Anomalies & Fire
	MOD13A2.006			16 day (2000-Present)	Terra Vegetation Indices
	MOD08_M3.006	1 arc		Monthly (2000 Present)	Terra Atmosphere

TABLE IV
CONTINUED

ASTER	*L1T radiance*	*15/ 30/ 90 m*	*Global*	*1 day (2000-Present)*	
	Global emissivity	*100 m*		*Once (2000-2008)*	
Topography	*Shuttle Radar Topography Mission*	*30 m*	*60°N–54°S*	*2000*	
	USGS National Elevation Dataset	*1/ 3 arc*	*United States*	*2012*	
	USGS GMTED2010	*7.5"arc*	*83°N–57°S*	*2010*	
	GTOPO30	*30"arc*	*Global*	*1996*	
	ETOPO1	*1' arc*	*Global*	*2008*	
	HYCOM	*0.08 arc*	*Global*	*Daily (1992-Present)*	*Hybrid Coordinate Ocean Model, Sea Surface Elevation*
	ALOS DSM	*30 m*	*Global*	*Once (2006-2011)*	
	CHILI index Continuous Heat-Insolation Load Index	*90 m*	*Global*	*Once (2006-2011)*	*ALOS-based*
		90 m	*Global*	*Once (2006-2011)*	*SRTM-based*
		10 m	*USA*	*Once (2006-2011)*	*NED DEM-based*
	Landforms Landform classes	*90 m*	*Global*	*Once (2006-2011)*	*ALOS-based*
		90 m	*Global*	*Once (2006-2011)*	*SRTM-based*
		10 m	*USA*	*Once (2006-2011)*	*NED DEM-based*
	mTPI: Multi-Scale Topographic Position Index	*270 m*	*Global*	*Once (2006-2011)*	*ALOS-based*
		270 m	*Global*	*Once (2006-2011)*	*SRTM-based*
		270 m	*USA*	*Once (2006-2011)*	*NED DEM-based*
	Topographic Diversity	*270 m*	*Global*	*Once (2006-2011)*	*ALOS-based*
		270 m	*Global*	*Once (2006-2011)*	*SRTM-based*
		90 m	*USA*	*Once (2006-2011)*	*NED DEM-based*
	US Lithology	*90 m*	*USA*	*Once (2006-2011)*	*parent material of soil on the surface*
	US Physiography	*90 m*	*USA*	*Once (2006-2011)*	
	US NED Physiographic Diversity	*270 m*	*USA*	*Once (2006-2011)*	
	CryoSat-2 DEM	*1 km*	*Antarctica*	*Once (2010-2016)*	
	AHN Netherlands DEM	*0.5 m*	*Netherlands*	*2012*	*Interpolated Non-Interpolated Raw Samples*
	Canadian Digital Elevation Model	*0.75 arc*	*Canada*	*Once (1945-2010)*	
	DEM-H	*1 arc*	*Australia*	*2010*	*Australian SRTM Hydrologically Enforced Digital Elevation Model*
	DEM-S	*1 arc*	*Australia*	*2010*	*Australian Smoothed Digital Elevation Model*
	Australian DEM	*5 m*	*Australia*	*2015*	
Landcover	*GlobCover*	*300 m*	*90°N–65°S*	*2009*	*Non-periodic*
	USGS National Landcover Database	*30 m*	*CONUS*	*(1992-2016)*	*Non-periodic*
	UMD global forest change	*1 arc*	*80°N–57°S*	*(2000-2018)*	*Annual*
	JRC global surface water	*30 m*	*78°N–60°S*	*(1984-2018)*	*Monthly*
	GLCF tree cover	*30 m*	*Global*	*(2000-2010)*	*5 year*
	USDA NASS cropland data layer	*30 m*	*CONUS*	*(1997-now)*	*Annual*
	GFSAD1000	*1 km*	*Global*	*Once (2010)*	
	Canada AAFC	*30 m*	*Canada*	*Yearly (2009-Present)*	*Annual Crop Inventory*
	Copernicus CORINE Land Cover	*100 m*	*Europe*	*5 images (1986-2018)*	*1990-2000-2006-2012-2018*
	CGLS-LC100	*100 m*	*Global*	*Once (2015)*	*Copernicus Global Land Cover Layers*
	CSP gHM	*1 km*	*Global*	*2016*	*Global Human Modification*
	PDSI	*2.5 arc*	*CONUS*	*10 day (1979-Present)*	*University of Idaho Palmer Drought Severity Index*
Weather, precipitation & atmosphere	*GPM: Global Precipitation Measurement*	*0.1 arc*	*Global*	*3h (2000– Present)*	
	TRMM 3B42 precipitation	*0.25 arc*	*50°N–50°S*	*3 h (1998-now)*	
	CHIRPS precipitation	*0.05 arc*	*50°N–50°S*	*1 day (1981–Present)*	
	PERSIANN-CDR	*0.25 arc*	*60°N–60°S*	*Daily (1983-Present)*	
	NLDAS-2	*0.125 arc*	*North America*	*1 h (1979– Present)*	
	GLDAS-2.0	*0.25 arc*	*Global*	*3 h (1948–2010)*	
	GLDAS-2.1	*0.25 arc*	*Global*	*3 h (2000–now)*	

TABLE IV
CONTINUED

	NCEP reanalysis	2.5 arc	Global	6 h (1948– Present)	
	ORNL DAYMET weather	1 km	North America	Annual (1980-Present)	
	GRIDMET	4 km	CONUS	1 day (1979–Present)	
	NCEP global forecast system	25 arc	Global	6 h (2015– Present)	
	NCEP climate forecast system	0.2 arc	Global	6 h (1979– Present)	
	WorldClim	30″arc	Global	12 images (1960–1990)	
	NEX downscaled climate projections	0.25 arc	North America	1 day (1950–2099)	
Population	WorldPop	100 m	2010–2015	5 year Multiple	
	GPWv4	30″arc	85°N–60°S	5 year (2000–2019)	
	GHSL: Global Human Settlement Layers	38 m	Global	(1975-2014)	Built-Up Grid 1975-1990-2000-2015 (P2016)
High Resolution	Planet SkySat MS	2 m (Pan 0.8)	Sample Tiles	(2014-2016)	
	Planet SkySat RGB	0.8 m	Sample Tiles	(2014-2016)	
	USDA NAIP	1 m	CONUS	Sub-annual (2003-2019)	Aerial imagery
Soil	SLGA	90 m	Australia	(1950-2013)	Soil and Landscape Grid of Australia
	GLDAS-2.1	0.25 arc	Global	1 day (2000-Present)	Global Land Data Assimilation System
	GLDAS-2.0	0.25 arc	Global	1 day (1948-2010)	Global Land Data Assimilation System
	NASA-USDA SMAP	0.25 arc	Global	3 day (2015-Present)	Global Soil Moisture Data
	NASA-USDA Global Soil Moisture Data	0.25 arc	Global	3 day (2010-Present)	
	OpenLandMap	250 m	Global	Once (1950-2017)	Soil bulk density Clay content Sand content Soil taxonomy great groups Soil organic carbon content Soil pH in H2O Soil texture class (USDA system) Soil water content
Snow	GLIMS			2016 2017	Global Land Ice Measurements from Space
	FLDAS	0.1 arc	Global	Monthly (1982 Present)	Famine Early Warning Systems
	Daymet V3	1 km	Global	Daily (1980-Present)	Daily Surface Weather and Climatological Summaries
	CFSR	0.2 arc	Global	6 h (1979- Present)	Climate Forecast System Reanalysis
	CFSV2	0.2 arc	Global	6 h (1979- Present)	NCEP Climate Forecast System Version 2
SAR	Forest/Non-Forest Map	25 m	Global	Once (2007-2017)	PALSAR-2/PALSAR Forest/Non-Forest Map
	PALSAR-2/PALSAR Mosaic	25 m	Global	Once (2007-2018)	
Rainfall	TRMM 3B42	0.25 arc	Global	3 h (1998- Present)	Precipitation Estimates
	TRMM 3B43	0.25 arc	Global	Monthly (1998-Present)	Precipitation Estimates
	KBDI	4 km	Global	Daily (2007-Present)	Keetch-Byram Drought Index
Others	NOAA CDR	0.25 arc	Global	3 h (1988- Present)	Ocean Near-Surface Atmospheric Properties
	PROBA-V top of canopy reflectance	100/300 m	Global	2 day (2013–Present)	
	EO-1 Hyperion hyperspectral radiance	30 m	Global	Targeted (2001–2017)	
	DMSP-OLS nighttime lights	30 arc	Global	Annual (1992–2013)	

REFERENCES

[1] M. Amani *et al.*, "Canadian wetland inventory using Google Earth Engine: The first map and preliminary results," *Remote Sens.*, vol. 11, no. 7, Apr. 2019, Art. no. 842.

[2] H. Tamiminia, B. Salehi, M. Mahdianpari, L. Quackenbush, S. Adeli, and B. Brisco, "Google Earth Engine for geo-big data applications: A meta-analysis and systematic review," *ISPRS J. Photogrammetry Remote Sens.*, vol. 164, pp. 152–170, Jun. 2020.

[3] M. Chi, A. Plaza, J. A. Benediktsson, Z. Sun, J. Shen, and Y. Zhu, "Big data for remote sensing: Challenges and opportunities," *Proc. IEEE*, vol. 104, no. 11, pp. 2207–2219, Nov. 2016.

[4] Y. Ma *et al.*, "Remote sensing big data computing: Challenges and opportunities," *Future Gener. Comput. Syst.*, vol. 51, pp. 47–60, Oct. 2015.

[5] B. Wilder, *Cloud Architecture Patterns: Using Microsoft Azure*. Newton, MA, USA: O'Reilly Media, 2012.

[6] N. Gorelick, M. Hancher, M. Dixon, S. Ilyushchenko, D. Thau, and R. Moore, "Google earth engine: Planetary-scale geospatial analysis for everyone," *Remote Sens. Environ.*, vol. 202, pp. 18–27, Dec. 2017.

[7] J. Hird, E. DeLancey, G. McDermid, and J. Kariyeva, "Google Earth Engine, open-access satellite data, and machine learning in support of large-area probabilistic wetland mapping," *Remote Sens.*, vol. 9, no. 12, Dec. 2017, Art. no. 1315.

[8] M. C. Hansen *et al.*, "High-resolution global maps of 21st-century forest cover change," *Science*, vol. 342, no. 6160, pp. 850–853, Nov. 2013.

[9] L. Kumar and O. Mutanga, "Google Earth Engine applications since inception: Usage, trends, and potential," *Remote Sens.*, vol. 10, no. 10, Sep. 2018, Art. no. 1509.

[10] O. Mutanga and L. Kumar, "Google Earth Engine applications," *Remote Sens*., vol. 11, no. 5, pp. 11–14, 2019.

[11] L. Bi, B. L. Fu, P. Q. Lou, and T. Y. Tang, "Delineation water of pearl river basin using Landsat images from Google Earth Engine," *ISPRS, Int. Arch. Photogrammetry Remote Sens. Spatial Inf. Sci.*, vol. XLII-3/W10, pp. 5–10, Feb. 2020, pp. 5–10.

[12] G. Mateo-García, L. Gómez-Chova, J. Amorós-López, J. Muñoz-Marí, and G. Camps-Valls, "Multitemporal cloud masking in the Google Earth Engine," *Remote Sens*., vol. 10, no. 7, Jul. 2018, Art. no. 1079.

[13] H. Li *et al.*, "A Google Earth Engine-enabled software for efficiently generating high-quality user-ready Landsat mosaic images," *Environ. Model. Softw.*, vol. 112, pp. 16–22, Feb. 2019.

[14] S. Xie, L. Liu, X. Zhang, J. Yang, X. Chen, and Y. Gao, "Automatic land-cover mapping using Landsat time-series data based on Google Earth Engine," *Remote Sens.*, vol. 11, no. 24, Dec. 2019, Art. no. 3023.

[15] J. Lee, J. Cardille, and M. Coe, "BULC-U: Sharpening resolution and improving accuracy of land-use/land-cover classifications in Google Earth Engine," *Remote Sens.*, vol. 10, no. 9, Sep. 2018, Art. no. 1455.

[16] M. Amani *et al.*, "A generalized supervised classification scheme to produce provincial wetland inventory maps: An application of Google Earth Engine for big geo data processing," *Big Earth Data*, vol. 3, no. 4, pp. 378–394, Oct. 2019.

[17] R. Ravanelli *et al.*, "Monitoring the impact of land cover change on surface urban heat island through Google Earth Engine: Proposal of a global methodology, first applications and problems," *Remote Sens*., vol. 10, no. 9, Sep. 2018, Art. no. 1488.

[18] P. Gong *et al.*, "Annual maps of global artificial impervious area (GAIA) between 1985 and 2018," *Remote Sens. Environ.*, vol. 236, Jan. 2020, Art. no. 111510.

[19] D. Mandal, V. Kumar, A. Bhattacharya, Y. S. Rao, P. Siqueira, and S. Bera, "Sen4Rice: A processing chain for differentiating early and late transplanted rice using time-series Sentinel-1 SAR data with Google Earth Engine," *IEEE Geosci. Remote Sens. Lett.*, vol. 15, no. 12, pp. 1947–1951, Dec. 2018.

[20] D. Traganos, D. Poursanidis, B. Aggarwal, N. Chrysoulakis, and P. Reinartz, "Estimating satellite-derived bathymetry (SDB) with the google earth engine and Sentinel-2," *Remote Sens.*, vol. 10, no. 6, Jun. 2018, Art. no. 859.

[21] M. Campos-Taberner *et al.*, "Global estimation of biophysical variables from Google Earth Engine platform," *Remote Sens.*, vol. 10, no. 8, Jul. 2018, Art. no. 1167.

[22] R. Xu and D. WunschII, "Survey of clustering algorithms," *IEEE Trans. Neural Netw.*, vol. 16, no. 3, pp. 645–678, May 2005.

[23] A. Ghorbanian and A. Mohammadzadeh, "An unsupervised feature extraction method based on band correlation clustering for hyperspectral image classification using limited training samples," *Remote Sens. Lett.*, vol. 9, no. 10, pp. 982–991, Oct. 2018.

[24] A. Moghimi, S. Khazai, and A. Mohammadzadeh, "An improved fast level set method initialized with a combination of k-means clustering and Otsu thresholding for unsupervised change detection from SAR images," *Arab. J. Geosci.*, vol. 10, no. 13, p. 293, Jul. 2017.

[25] T. Calinski and J. Harabasz, "A dendrite method for cluster analysis," *Commun. Statist., Theory Methods*, vol. 3, no. 1, pp. 1–27, 1974.

[26] A. W. M. Dan Pelleg, "X-means: Extending k-means with efficient estimation of the number of clusters," in *Proc. 17th Int. Conf. Mach. Learning*, 2000, pp. 727–734.

[27] J. H. Gennari, P. Langley, and D. Fisher, "Models of incremental concept formation," *Artif. Intell.*, vol. 40, nos. 1–3, pp. 11–61, Sep. 1989.

[28] R. Achanta and S. Susstrunk, "Superpixels and polygons using simple non-iterative clustering," in *Proc. IEEE Conf. Comput. Vis. Pattern Recognit.*, Jul. 2017, pp. 4895–4904.

[29] M. Mahdianpari, B. Salehi, F. Mohammadimanesh, S. Homayouni, and E. Gill, "The first wetland inventory map of Newfoundland at a spatial resolution of 10 m using Sentinel-1 and Sentinel-2 data on the Google Earth Engine cloud computing platform," *Remote Sens*., vol. 11, no. 1, Dec. 2018, Art. no. 43.

[30] Z. Zhu and C. E. Woodcock, "Continuous change detection and classification of land cover using all available Landsat data," *Remote Sens. Environ.*, vol. 144, pp. 152–171, Mar. 2014.

[31] E. B. Brooks, R. H. Wynne, V. A. Thomas, C. E. Blinn, and J. W. Coulston, "On-the-Fly massively multitemporal change detection using statistical quality control charts and Landsat data," *IEEE Trans. Geosci. Remote Sens.*, vol. 52, no. 6, pp. 3316–3332, Jun. 2014.

[32] R. E. Kennedy, Z. Yang, and W. B. Cohen, "Detecting trends in forest disturbance and recovery using yearly Landsat time series: 1. LandTrendr — Temporal segmentation algorithms," *Remote Sens. Environ.*, vol. 114, no. 12, pp. 2897–2910, Dec. 2010.

[33] C. Huang, S. N. Goward, J. G. Masek, N. Thomas, Z. Zhu, and J. E. Vogelmann, "An automated approach for reconstructing recent forest disturbance history using dense Landsat time series stacks," *Remote Sens. Environ.*, vol. 114, no. 1, pp. 183–198, Jan. 2010.

[34] M. Hughes, S. Kaylor, and D. Hayes, "Patch-based forest change detection from Landsat time series," *Forests*, vol. 8, no. 5, May 2017, Art. no. 166.

[35] A. M. Shew and A. Ghosh, "Using multi-temporal remote sensing data to analyze the spatio-temporal patterns of dry season rice production in Bangladesh," *ISPRS Ann. Photogrammetry Remote Sens. Spatial Inf. Sci.*, vol. IV-4/W2, pp. 61–68, Oct. 2017.

[36] D. Parastatidis, Z. Mitraka, N. Chrysoulakis, and M. Abrams, "Online global land surface temperature estimation from Landsat," *Remote Sens*., vol. 9, no. 12, Nov. 2017, Art. no. 1208.

[37] Z. Yang, W. Li, Q. Chen, S. Wu, S. Liu, and J. Gong, "A scalable cyberinfrastructure and cloud computing platform for forest aboveground biomass estimation based on the Google Earth Engine," *Int. J. Digit. Earth*, vol. 12, no. 9, pp. 995–1012, Sep. 2019.

[38] H. Xu and Y. Bai, "Evaluation of urban lake evolution using Google Earth Engine—A case study of Wuhan, China," in *Proc. 4th Int. Conf. Agro-Geoinformat.,* Jul. 2015, pp. 322–325.

[39] I. Fuentes, J. Padarian, F. van Ogtrop, and R. W. Vervoort, "Comparison of surface water volume estimation methodologies that couple surface reflectance data and digital terrain models," *Water*, vol. 11, no. 4, Apr. 2019, Art. no. 780.

[40] S. S. Ray, "Exploring machine learning classification algorithms for crop classification using Sentinel 2 data," *ISPRS, Int. Arch. Photogrammetry Remote Sens. Spatial Inf. Sci.*, vol. XLII-3/W6, pp. 573–578, Jul. 2019.

[41] "Python vs. Javascript APIs." [Online]. Available: https://developers.google.com/earth-engine/python_install. Accesed: Jan. 2020.

[42] "GEE developers forum." [Online]. Available: https://developers.google.com/earth-engine/

[43] "GEE Python API Docs." [Online]. Available: ttps://colab.research.google.com/github/csaybar/EEwPython/blob/dev/1_Introduction.ipynb#scrollTo=9CRoDhQNiHC8, Accesed: Jan. 2020.

[44] A. F. Sunar, N. Yagmur, and A. Dervisoglu, "Flood analysis with remote sensing data – A case study: Maritsa river, Edirne," *ISPRS, Int. Arch. Photogrammetry Remote Sens. Spatial Inf. Sci.*, vol. XLII-3/W8, pp. 497–502, Aug. 2019.

[45] E. Çolak, M. Chandra, and F. Sunar, "The use of multi-temporal Sentinel satellites in the analysis of land cover/land use changes caused by the nuclear power plant construction," *ISPRS, Int. Arch. Photogrammetry Remote Sens. Spatial Inf. Sci.*, vol. XLII-3/W8, pp. 491–495, Aug. 2019.

[46] M. Di Tullio, F. Nocchi, A. Camplani, N. Emanuelli, A. Nascetti, and M. Crespi, "Copernicus big data and Google Earth Engine for glacier surface velocity field monitoring: Feasibility demonstration on San Rafael and San Quintin glaciers," *ISPRS, Int. Arch. Photogrammetry Remote Sens. Spatial Inf. Sci.*, vol. XLII–3, pp. 289–294, Apr. 2018.

[47] TFrecord and Earth Engine. [Online]. Available: https://developers.google.com/earth-engine/tfrecord, Accesed: Jan. 2020.

[48] E. R. DeLancey, J. F. Simms, M. Mahdianpari, B. Brisco, C. Mahoney, and J. Kariyeva, "Comparing deep learning and shallow learning for large-scale wetland classification in Alberta, Canada," *Remote Sens.*, vol. 12, no. 1, Dec. 2019, Art. no. 2.

[49] L. Parente, E. Taquary, A. Silva, C. Souza, and L. Ferreira, "Next generation mapping: Combining deep learning, cloud computing, and big remote sensing data," *Remote Sens.*, vol. 11, no. 23, Dec. 2019, Art. no. 2881.

[50] J. Padarian, B. Minasny, and A. B. McBratney, "Using Google's cloud-based platform for digital soil mapping," *Comput. Geosci.*, vol. 83, pp. 80–88, Oct. 2015.

[51] "Sentinel-1 algorithms." [Online]. Available: https://developers.google.com/earth-engine/sentinel1

[52] F. Keller, J. Sänger, T. Kersten, and J. Schiewe, "Historical 4D city model of the free and Hanseatic city of Hamburg – automated generation and presentation within the Google Earth Engine," *Photogrammtrie Fernerkundung, Geoinf.*, vol. 2011, no. 3, pp. 155–169, Jun. 2011.

[53] M. Amani and M. R. Mobasheri, "A parametric method for estimation of leaf area index using Landsat ETM+ data," *GIScience Remote Sens.*, vol. 52, no. 4, pp. 478–497, Jul. 2015.

[54] B. Smith *et al.*, "Implications of incorporating N cycling and N limitations on primary production in an individual-based dynamic vegetation model," *Biogeosciences*, vol. 11, no. 7, pp. 2027–2054, Apr. 2014.

[55] T. G. Workie and H. J. Debella, "Climate change and its effects on vegetation phenology across ecoregions of Ethiopia," *Glob. Ecol. Conservation*, vol. 13, Jan. 2018, Art. no. e00366.

[56] S. Besnard *et al.*, "Memory effects of climate and vegetation affecting net ecosystem CO_2 fluxes in global forests," *PLoS One*, vol. 14, no. 2, Feb. 2019, Art. no. e0211510.

[57] B. G. Peter and J. P. Messina, "Errors in time-series remote sensing and an open access application for detecting and visualizing spatial data outliers using Google Earth Engine," *IEEE J. Sel. Topics Appl. Earth Obs. Remote Sens.*, vol. 12, no. 4, pp. 1165–1174, Apr. 2019.

[58] M. Zhang, P. Gong, S. Qi, C. Liu, and T. Xiong, "Mapping bamboo with regional phenological characteristics derived from dense Landsat time series using Google Earth Engine," *Int. J. Remote Sens.*, vol. 40, no. 24, pp. 9541–9555, Dec. 2019.

[59] Z. Xie *et al.*, "Using Landsat observations (1988–2017) and Google Earth Engine to detect vegetation cover changes in rangelands—A first step towards identifying degraded lands for conservation," *Remote Sens. Environ.*, vol. 232, Oct. 2019, Art. no. 111317.

[60] J. Pei *et al.*, "Time series of Landsat imagery shows vegetation recovery in two fragile karst watersheds in Southwest China from 1988 to 2016," *Remote Sens.*, vol. 11, no. 17, Aug. 2019, Art. no. 2044.

[61] C. D. Mendenhall and A. M. Wrona, "Improving tree cover estimates for fine-scale landscape ecology," *Landscape Ecol.*, vol. 33, no. 10, pp. 1691–1696, Oct. 2018.

[62] E. L. Bullock, C. E. Woodcock, and P. Olofsson, "Monitoring tropical forest degradation using spectral unmixing and Landsat time series analysis," *Remote Sens. Environ.*, vol. 238, Mar. 2020, Art. no. 110968.

[63] F. Ramdani, "Recent expansion of oil palm plantation in the most eastern part of Indonesia: feature extraction with polarimetric SAR," *Int. J. Remote Sens.*, vol. 40, no. 19, pp. 7371–7388, Oct. 2019.

[64] K. Anderson, D. Fawcett, A. Cugulliere, S. Benford, D. Jones, and R. Leng, "Vegetation expansion in the subnival Hindu Kush Himalaya," *Glob. Change Biol.*, vol. 26, no. 3, pp. 1608–1625, Mar. 2020.

[65] B. Cao, G. M. Domke, M. B. Russell, and B. F. Walters, "Spatial modeling of litter and soil carbon stocks on forest land in the conterminous United States," *Sci. Total Environ.*, vol. 654, pp. 94–106, Mar. 2019.

[66] J. Pérez-Romero, R. M. Navarro-Cerrillo, G. Palacios-Rodriguez, C. Acosta, and F. J. Mesas-Carrascosa, "Improvement of remote sensing-based assessment of defoliation of *Pinus* spp. caused by *Thaumetopoea Pityocampa* Denis and Schiffermüller and related environmental drivers in Southeastern Spain," *Remote Sens.*, vol. 11, no. 14, Jul. 2019, Art. no. 1736.

[67] C. Wei, D. N. Karger, and A. M. Wilson, "Spatial detection of alpine treeline ecotones in the Western United States," *Remote Sens. Environ.*, vol. 240, Apr. 2020, Art. no. 111672.

[68] K. Shimizu, T. Ota, and N. Mizoue, "Detecting forest changes using dense Landsat 8 and Sentinel-1 time series data in tropical seasonal forests," *Remote Sens.*, vol. 11, no. 16, Aug. 2019, Art. no. 1899.

[69] L. Parente, V. Mesquita, F. Miziara, L. Baumann, and L. Ferreira, "Assessing the pasturelands and livestock dynamics in Brazil, from 1985 to 2017: A novel approach based on high spatial resolution imagery and Google Earth Engine cloud computing," *Remote Sens. Environ.*, vol. 232, Oct. 2019, Art. no. 111301.

[70] M. O. Jones *et al.*, "Innovation in rangeland monitoring: annual, 30 m, plant functional type percent cover maps for U.S. rangelands, 1984-2017," *Ecosphere*, vol. 9, no. 9, Sep. 2018, Art. no. e02430.

[71] V. Jansen, C. Kolden, and H. Schmalz, "The development of near real-time biomass and cover estimates for adaptive rangeland management using Landsat 7 and Landsat 8 surface reflectance products," *Remote Sens.*, vol. 10, no. 7, Jul. 2018, Art. no. 1057.

[72] S. Xu, G. Li, and Z. Li, "China agricultural outlook for 2015–2024 based on China Agricultural Monitoring and Early-warning System (CAMES)," *J. Integrative Agriculture*, vol. 14, no. 9, pp. 1889–1902, Sep. 2015.

[73] J. Schindler, F. Graef, H. J. König, and D. Mchau, "Developing community-based food security criteria in rural Tanzania," *Food Secur.*, vol. 9, no. 6, pp. 1285–1298, Dec. 2017.

[74] J. W. McArthur and J. D. Sachs, "Agriculture, aid, and economic growth in Africa," *World Bank Econ. Rev.*, vol. 33, no. 1, pp. 1–20, Feb. 2019.

[75] P. Han, J. Chen, Y. Han, L. Yi, Y. Zhang, and X. Jiang, "Monitoring rubber plantation distribution on Hainan Island using Landsat OLI imagery," *Int. J. Remote Sens.*, vol. 39, no. 8, pp. 2189–2206, Apr. 2018.

[76] A. Poortinga *et al.*, "Mapping plantations in Myanmar by fusing Landsat-8, Sentinel-2 and Sentinel-1 data along with systematic error quantification," *Remote Sens.*, vol. 11, no. 7, Apr. 2019, Art. no. 831.

[77] H. Tian, N. Huang, Z. Niu, Y. Qin, J. Pei, and J. Wang, "Mapping winter crops in China with multi-source satellite imagery and phenology-based algorithm," *Remote Sens.*, vol. 11, no. 7, Apr. 2019, Art. no. 820.

[78] G. Ghazaryan *et al.*, "A rule-based approach for crop identification using multi-temporal and multi-sensor phenological metrics," *Eur. J. Remote Sens.*, vol. 51, no. 1, pp. 511–524, Jan. 2018.

[79] L. Liang, B. R. K. Runkle, B. B. Sapkota, and M. L. Reba, "Automated mapping of rice fields using multi-year training sample normalization," *Int. J. Remote Sens.*, vol. 40, no. 18, pp. 7252–7271, Sep. 2019.

[80] S. Wang, G. Azzari, and D. B. Lobell, "Crop type mapping without field-level labels: Random forest transfer and unsupervised clustering techniques," *Remote Sens. Environ.*, vol. 222, pp. 303–317, Mar. 2019.

[81] F. Rembold *et al.*, "ASAP: A new global early warning system to detect anomaly hot spots of agricultural production for food security analysis," *Agricultural Syst.*, vol. 168, pp. 247–257, Jan. 2019.

[82] M. Rudiyanto, S. Minasny, R. M. Shah, N. C. Soh, C. Arif, and B. I. Setiawan, "Automated near-real-time mapping and monitoring of rice extent, cropping patterns, and growth stages in Southeast Asia using Sentinel-1 time series on a Google Earth Engine platform," *Remote Sens.*, vol. 11, no. 14, Jul. 2019, Art. no. 1666.

[83] Z. Jin *et al.*, "Smallholder maize area and yield mapping at national scales with Google Earth Engine," *Remote Sens. Environ.*, vol. 228, pp. 115–128, Jul. 2019.

[84] D. B. Lobell, D. Thau, C. Seifert, E. Engle, and B. Little, "A scalable satellite-based crop yield mapper," *Remote Sens. Environ.*, vol. 164, pp. 324–333, Jul. 2015.

[85] J. M. Deines, A. D. Kendall, and D. W. Hyndman, "Annual irrigation dynamics in the U.S. Northern High Plains derived from Landsat satellite data," *Geophys. Res. Lett.*, vol. 44, no. 18, pp. 9350–9360, Sep. 2017.

[86] S. Ragettli, T. Herberz, and T. Siegfried, "An unsupervised classification algorithm for multi-temporal irrigated area mapping in central Asia," *Remote Sens.*, vol. 10, no. 11, Nov. 2018, Art. no. 1823.

[87] S. G. Yalew, A. van Griensven, and P. van der Zaag, "AgriSuit: A web-based GIS-MCDA framework for agricultural land suitability assessment," *Comput. Electron. Agriculture*, vol. 128, pp. 1–8, Oct. 2016.

[88] N. You and J. Dong, "Examining earliest identifiable timing of crops using all available Sentinel 1/2 imagery and Google Earth Engine," *ISPRS J. Photogrammetry Remote Sens.*, vol. 161, pp. 109–123, Mar. 2020.

[89] F. Yao, J. Wang, C. Wang, and J.-F. Crétaux, "Constructing long-term high-frequency time series of global lake and reservoir areas using Landsat imagery," *Remote Sens. Environ.*, vol. 232, Oct. 2019, Art. no. 111210.

[90] D. Scherler, H. Wulf, and N. Gorelick, "Global assessment of supraglacial debris-cover extents," *Geophys. Res. Lett.*, vol. 45, no. 21, pp. 11798–11805, Nov. 2018.

[91] T. Tedesche, E. D. Trochin, S. R. Fassnacht, and G. J. Wolken, "Extent changes in the perennial snowfields of gates of the Arctic national park and preserve, Alaska," *Hydrology*, vol. 6, no. 2, Jun. 2019, Art. no. 53.

[92] B. Snapir, A. Momblanch, S. K. Jain, T. W. Waine, and I. P. Holman, "A method for monthly mapping of wet and dry snow using Sentinel-1 and MODIS: Application to a Himalayan river basin," *Int. J. Appl. Earth Observ. Geoinf.*, vol. 74, pp. 222–230, Feb. 2019.

[93] U. N. T. Nguyen, L. T. H. Pham, and T. D. Dang, "An automatic water detection approach using Landsat 8 OLI and Google Earth Engine cloud computing to map lakes and reservoirs in New Zealand," *Environmental Monitoring Assessment*, vol. 191, no. 4, Apr. 2019, Art. no. 235.

[94] Y. Zhou *et al.*, "Continuous monitoring of lake dynamics on the Mongolian Plateau using all available Landsat imagery and Google Earth Engine," *Sci. Total Environ.*, vol. 689, pp. 366–380, Nov. 2019.

[95] T. Sagawa, Y. Yamashita, T. Okumura, and T. Yamanokuchi, "Satellite Derived Bathymetry using machine learning and multi-temporal satellite images," *Remote Sens.*, vol. 11, no. 10, May 2019, Art. no. 1155.

[96] K. Vos, M. D. Harley, K. D. Splinter, J. A. Simmons, and I. L. Turner, "Sub-annual to multi-decadal shoreline variability from publicly available satellite imagery," *Coastal Eng.*, vol. 150, pp. 160–174, Aug. 2019.

[97] W. Cao, Y. Zhou, R. Li, and X. Li, "Mapping changes in coastlines and tidal flats in developing islands using the full time series of Landsat images," *Remote Sens. Environ.*, vol. 239, Mar. 2020, Art. no. 111665.

[98] F. Chen, M. Zhang, B. Tian, and Z. Li, "Extraction of glacial lake outlines in Tibet plateau using Landsat 8 imagery and Google Earth Engine," *IEEE J. Sel. Topics Appl. Earth Obs. Remote Sens.*, vol. 10, no. 9, pp. 4002–4009, Sep. 2017.

[99] S. Murphy, R. Wright, and D. Rouwet, "Color and temperature of the crater lakes at Kelimutu volcano through time," *Bull. Volcanol.*, vol. 80, no. 1, Jan. 2018, Art. no. 2.

[100] M. Zhang, F. Chen, and B. Tian, "An automated method for glacial lake mapping in High Mountain Asia using Landsat 8 imagery," *J. Mountain Sci.*, vol. 15, no. 1, pp. 13–24, Jan. 2018.

[101] N. E. Wayand, C. B. Marsh, J. M. Shea, and J. W. Pomeroy, "Globally scalable alpine snow metrics," *Remote Sens. Environ.*, vol. 213, pp. 61–72, Aug. 2018.

[102] C. G. Griffin, J. W. McClelland, K. E. Frey, G. Fiske, and R. M. Holmes, "Quantifying CDOM and DOC in major Arctic rivers during ice-free conditions using Landsat TM and ETM+ data," *Remote Sens. Environ.*, vol. 209, pp. 395–409, May 2018.

[103] Z. Cao, R. Ma, H. Duan, K. Xue, and M. Shen, "Effect of satellite temporal resolution on long-term suspended particulate matter in inland lakes," *Remote Sens.*, vol. 11, no. 23, Nov. 2019, Art. no. 2785.

[104] E. Medina-Lopez and L. Ureña-Fuentes, "High-resolution sea surface temperature and salinity in the global ocean from raw satellite data," *Remote Sens.*, vol. 11, no. 19, Sep. 2019, Art. no. 2191.

[105] S. Lin, L. N. Novitski, J. Qi, and R. J. Stevenson, "Landsat TM/ETM+ and machine-learning algorithms for limnological studies and algal bloom management of inland lakes," *J. Appl. Remote Sens.*, vol. 12, no. 02, Apr. 2018, Art. no. 1.

[106] S. Meerow, J. P. Newell, and M. Stults, "Defining urban resilience: A review," *Landscape Urban Planning*, vol. 147, pp. 38–49, Mar. 2016.

[107] S. A. Ahmadi, A. Ghorbanian, and A. Mohammadzadeh, "Moving vehicle detection, tracking and traffic parameter estimation from a satellite video: A perspective on a smarter city," *Int. J. Remote Sens.*, vol. 40, no. 22, pp. 8379–8394, Nov. 2019.

[108] Q. Zhong, J. Ma, B. Zhao, X. Wang, J. Zong, and X. Xiao, "Assessing spatial-temporal dynamics of urban expansion, vegetation greenness and photosynthesis in megacity Shanghai, China during 2000–2016," *Remote Sens. Environ.*, vol. 233, Nov. 2019, Art no. 111374.

[109] S. Parsian and M. Amani, "Building extraction from fused LiDAR and hyperspectral data using Random Forest Algorithm," *GEOMATICA*, vol. 71, no. 4, pp. 185–193, Dec. 2017.

[110] M. Ranagalage and S. Dissanayake, "The Impacts of landscape changes on annual mean land surface temperature in the tropical mountain city of Sri Lanka: A case study of Nuwara Eliya (1996–2017)," *Sustainability*, vol. 11, no. 19, Oct. 2019, Art. no. 5517.

[111] D. Liu, N. Chen, X. Zhang, C. Wang, and W. Du, "Annual large-scale urban land mapping based on Landsat time series in Google Earth Engine and OpenStreetMap data: A case study in the middle Yangtze River basin," *ISPRS J. Photogrammetry Remote Sens.*, vol. 159, pp. 337–351, Jan. 2020.

[112] M. Demuzere, B. Bechtel, and G. Mills, "Global transferability of local climate zone models," *Urban Climate*, vol. 27, pp. 46–63, Mar. 2019.

[113] A. Middel, J. Lukasczyk, R. Maciejewski, M. Demuzere, and M. Roth, "Sky view factor footprints for urban climate modeling," *Urban Climate*, vol. 25, pp. 120–134, Sep. 2018.

[114] Q. Duan, M. Tan, Y. Guo, X. Wang, and L. Xin, "Understanding the spatial distribution of urban forests in china using Sentinel-2 images with google earth engine," *Forests*, vol. 10, no. 9, Aug. 2019, Art. no. 729.

[115] C. Huang, J. Yang, and P. Jiang, "Assessing impacts of urban form on landscape structure of urban green spaces in China using Landsat images based on Google Earth Engine," *Remote Sens.*, vol. 10, no. 10, Oct. 2018, Art. no. 1569.

[116] A. G. Auffret, A. Kimberley, J. Plue, and E. Waldén, "Super-regional land-use change and effects on the grassland specialist flora," *Nature Commun.*, vol. 9, no. 1, Dec. 2018, Art. no. 3464.

[117] S. Mahdavi, B. Salehi, J. Granger, M. Amani, B. Brisco, and W. Huang, "Remote sensing for wetland classification: A comprehensive review," *GIScience Remote Sens.*, vol. 55, no. 5, pp. 623–658, Sep. 2018.

[118] A. Midekisa *et al.*, "Mapping land cover change over continental Africa using Landsat and Google Earth Engine cloud computing," *PLoS One*, vol. 12, no. 9, Sep. 2017, Art. no. e0184926.

[119] N. J. Murray, D. A. Keith, D. Simpson, J. H. Wilshire, and R. M. Lucas, "Remap: An online remote sensing application for land cover classification and monitoring," *Methods Ecol. Evol.*, vol. 9, no. 9, pp. 2019–2027, Sep. 2018.

[120] J. Miettinen, C. Shi, and S. C. Liew, "Towards automated 10–30 m resolution land cover mapping in insular South-East Asia," *Geocarto Int.*, vol. 34, no. 4, pp. 443–457, Mar. 2019.

[121] Y. Ge *et al.*, "Mapping annual land use changes in China's poverty-stricken areas from 2013 to 2018," *Remote Sens. Environ.*, vol. 232, Oct. 2019, Art. no. 111285.

[122] Y. Zhou *et al.*, "Are there sufficient Landsat observations for retrospective and continuous monitoring of land cover changes in China?," *Remote Sens.*, vol. 11, no. 15, Aug. 2019, Art. no. 1808.

[123] X. Wang *et al.*, "Tracking annual changes of coastal tidal flats in China during 1986–2016 through analyses of Landsat images with Google Earth Engine," *Remote Sens. Environ.*, vol. 238, Mar. 2020, Art. no. 110987.

[124] G. Muthusankar *et al.*, "When socio-economic plans exacerbate vulnerability to physical coastal processes on the South East coast of India," *J. Coastal Res.*, vol. 85, pp. 1446–1450, May 2018.

[125] Q. Wu *et al.*, "Integrating LiDAR data and multi-temporal aerial imagery to map wetland inundation dynamics using Google Earth Engine," *Remote Sens. Environ.*, vol. 228, pp. 1–13, Jul. 2019.

[126] A. Ghorbanian, M. Kakooei, M. Amani, S. Mahdavi, A. Mohammadzadeh, and M. Hasanlou, "Improved land cover map of Iran using Sentinel imagery within Google Earth Engine and a novel automatic workflow for land cover classification using migrated training samples," *ISPRS J. Photogrammetry Remote Sens.*, vol. 167, pp. 276–288, Sep. 2020.

[127] Y. Bayissa, T. Tadesse, G. Demisse, and A. Shiferaw, "Evaluation of satellite-based rainfall estimates and application to monitor meteorological drought for the Upper Blue Nile Basin, Ethiopia," *Remote Sens.*, vol. 9, no. 7, Jun. 2017, Art. no. 669.

[128] M. Amani, B. Salehi, S. Mahdavi, A. Masjedi, and S. Dehnavi, "Temperature-Vegetation-soil Moisture Dryness Index (TVMDI)," *Remote Sens. Environ.*, vol. 197, pp. 1–14, Aug. 2017.

[129] R. Khan, H. Gilani, N. Iqbal, and I. Shahid, "Satellite-based (2000–2015) drought hazard assessment with indices, mapping, and monitoring of Potohar plateau, Punjab, Pakistan," *Environ. Earth Sci.*, vol. 79, no. 1, Jan. 2020, Art. no. 23.

[130] L. J. Roberts, R. Burnett, J. Tietz, and S. Veloz, "Recent drought and tree mortality effects on the avian community in southern Sierra Nevada: A glimpse of the future?," *Ecol. Appl.*, vol. 29, no. 2, Mar. 2019, Art. no. e01848.

[131] K. Uddin, M. A. Matin, and F. J. Meyer, "Operational flood mapping using multi-temporal Sentinel-1 SAR images: A case study from Bangladesh," *Remote Sens.*, vol. 11, no. 13, Jul. 2019, Art. no. 1581.

[132] D. Amitrano, R. Guida, and G. Ruello, "Multitemporal SAR RGB processing for Sentinel-1 GRD products: Methodology and applications," *IEEE J. Sel. Topics Appl. Earth Obs. Remote Sens.*, vol. 12, no. 5, pp. 1497–1507, May 2019.

[133] T. Long *et al.*, "30 m resolution global annual burned area mapping based on Landsat Images and Google Earth Engine," *Remote Sens.*, vol. 11, no. 5, Feb. 2019, Art. no. 489.

[134] P. Sarricolea *et al.*, "Recent wildfires in central Chile: Detecting links between burned areas and population exposure in the wildland urban interface," *Sci. Total Environ.*, vol. 706, Mar. 2020, Art. no. 135894.

[135] B. Yu, F. Chen, and S. Muhammad, "Analysis of satellite-derived landslide at Central Nepal from 2011 to 2016," *Environ. Earth Sci.*, vol. 77, no. 9, May 2018, Art. no. 331.

[136] M. Kakooei and Y. Baleghi, "A two-level fusion for building irregularity detection in post-disaster VHR oblique images," *Earth Sci. Informat.*, vol. 13, pp. 459–477, Feb. 2020.

[137] E. Meilianda *et al.*, "Assessment of post-tsunami disaster land use/land cover change and potential impact of future sea-level rise to low-lying coastal areas: A case study of Banda Aceh coast of Indonesia," *Int. J. Disaster Risk Reduction*, vol. 41, Dec. 2019, Art. no. 101292.

[138] B. Hao *et al.*, "Land use change and climate variation in the three gorges reservoir catchment from 2000 to 2015 based on the Google Earth Engine," *Sensors*, vol. 19, no. 9, May 2019, Art. no. 2118.

[139] J.-C. Yeh and C.-H. Liao, "Impact of population and economic growth on carbon emissions in Taiwan using an analytic tool STIRPAT," *Sustain. Environ. Res.*, vol. 27, no. 1, pp. 41–48, Jan. 2017.

[140] I. R. Orimoloye, S. P. Mazinyo, A. M. Kalumba, O. Y. Ekundayo, and W. Nel, "Implications of climate variability and change on urban and human health: A review," *Cities*, vol. 91, pp. 213–223, Aug. 2019.

[141] H. Gu, Y. Cao, E. Elahi, and S. K. Jha, "Human health damages related to air pollution in China," *Environ. Sci. Pollut. Res.*, vol. 26, no. 13, pp. 13115–13125, May 2019.

[142] M. Fuentes, K. Millard, and E. Laurin, "Big geospatial data analysis for Canada's Air Pollutant Emissions Inventory (APEI): using google earth engine to estimate particulate matter from exposed mine disturbance areas," *GIScience Remote Sens.*, vol. 57, no. 2, pp. 245–257, Feb. 2020.

[143] W. Chen, H. Wang, H. Zhao, and K. Qin, "Google Earth Engine–assisted black carbon radiative forcing calculation over a heavy industrial city in China," *Air Quality Atmosphere Health*, vol. 13, no. 3, pp. 329–338, Mar. 2020.

[144] J. L. Huntington *et al.*, "Climate Engine: Cloud computing and visualization of climate and remote sensing data for advanced natural resource monitoring and process understanding," *Bull. Amer. Meteorological Soc.*, vol. 98, no. 11, pp. 2397–2410, Nov. 2017.

[145] T. Klein, M. Nilsson, A. Persson, and B. Håkansson, "From open data to open analyses—New opportunities for environmental applications?" *Environments*, vol. 4, no. 2, Apr. 2017, Art. no. 32.

[146] S. J. Weber, D. R. Mishra, S. B. Wilde, and E. Kramer, "Risks for cyanobacterial harmful algal blooms due to land management and climate interactions," *Sci. Total Environ.*, vol. 703, Feb. 2020, Art. no. 134608.

[147] E. Walker and V. Venturini, "Land surface evapotranspiration estimation combining soil texture information and global reanalysis datasets in Google Earth Engine," *Remote Sens. Lett.*, vol. 10, no. 10, pp. 929–938, Oct. 2019.

[148] H. Zeng *et al.*, "Spatiotemporal analysis of precipitation in the sparsely gauged Zambezi river basin using remote sensing and Google Earth Engine," *Remote Sens.*, vol. 11, no. 24, Dec. 2019, Art. no. 2977.

[149] L. Gómez-Chova, J. Amorós-López, G. Mateo-García, J. Muñoz-Marí, and G. Camps-Valls, "Cloud masking and removal in remote sensing image time series," *J. Appl. Remote Sens.*, vol. 11, no. 1, Jan. 2017, Art. no. 015005.

[150] D. Kong, Y. Zhang, X. Gu, and D. Wang, "A robust method for reconstructing global MODIS EVI time series on the Google Earth Engine," *ISPRS J. Photogrammetry Remote Sens.*, vol. 155, pp. 13–24, Sep. 2019.

[151] R. Chastain, I. Housman, J. Goldstein, M. Finco, and K. Tenneson, "Empirical cross sensor comparison of Sentinel-2A and 2B MSI, Landsat-8 OLI, and Landsat-7 ETM+ top of atmosphere spectral characteristics over the conterminous United States," *Remote Sens. Environ.*, vol. 221, pp. 274–285, Feb. 2019.

[152] M. N. Hasan, M. Shrestha, L. Leigh, and D. Helder, "Evaluation of an Extended PICS (EPICS) for calibration and stability monitoring of optical satellite sensors," *Remote Sens.*, vol. 11, no. 15, Jul. 2019, Art. no. 1755.

[153] H. Huang, J. Wang, C. Liu, L. Liang, C. Li, and P. Gong, "The migration of training samples towards dynamic global land cover mapping," *ISPRS J. Photogrammetry Remote Sens.*, vol. 161, pp. 27–36, Mar. 2020.

[154] M. Kakooei, A. Nascetti, and Y. Ban, "Sentinel-1 global coverage foreshortening mask extraction: An open source implementation based on Google Earth Engine," in *Proc. IEEE Int. Geosci. Remote Sens. Symp.*, Jul. 2018, pp. 6836–6839.

[155] R. Lal, J. Kimble, and R. F. Follett, "Pedospheric processes and the carbon cycle," in *Soil Processes and the Carbon Cycle*. Boca Raton, FL, USA: CRC Press, 2018, pp. 1–8.

[156] G. Tóth, T. Hermann, M. R. da Silva, and L. Montanarella, "Monitoring soil for sustainable development and land degradation neutrality," *Environmental Monitoring Assessment*, vol. 190, no. 2, Feb. 2018, Art. no. 57.

[157] H.-J. Vogel *et al.*, "A systemic approach for modeling soil functions," *SOIL*, vol. 4, no. 1, pp. 83–92, Mar. 2018.

[158] A. Ghorbanian, M. R. Sahebi, and A. Mohammadzadeh, "Optimization approach to retrieve soil surface parameters from single-acquisition single-configuration SAR data," *Comptes Rendus Geosci.*, vol. 351, no. 4, pp. 332–339, Apr. 2019.

[159] S. M. MirMazloumi and M. R. Sahebi, "Assessment of different backscattering models for bare soil surface parameters estimation from SAR data in band C, L and P," *Eur. J. Remote Sens.*, vol. 49, no. 1, pp. 261–278, Jan. 2016.

[160] H. R. Mirsoleimani, M. R. Sahebi, N. Baghdadi, and M. El Hajj, "Bare soil surface moisture retrieval from Sentinel-1 SAR data based on the calibrated IEM and Dubois models using neural networks," *Sensors*, vol. 19, no. 14, Jul. 2019, Art. no. 3209.

[161] R. R. Poppiel *et al.*, "Mapping at 30 m resolution of soil attributes at multiple depths in midwest Brazil," *Remote Sens.*, vol. 11, no. 24, Dec. 2019, Art. no. 2905.

[162] A. A. Pericak *et al.*, "Mapping the yearly extent of surface coal mining in Central Appalachia using Landsat and Google Earth Engine," *PLoS One*, vol. 13, no. 7, Jul. 2018, Art. no. e0197758.

[163] E. Sun, A. Nieto, and Z. Li, "GPS and Google Earth based 3D assisted driving system for trucks in surface mines," *Mining Sci. Technol.*, vol. 20, no. 1, pp. 138–142, Jan. 2010.

[164] S. A. S. Brooke, M. D'Arcy, P. J. Mason, and A. C. Whittaker, "Rapid multispectral data sampling using Google Earth Engine," *Comput. Geosci.*, vol. 135, Feb. 2020, Art. no. 104366.

[165] H. A. Orengo and C. A. Petrie, "Multi-scale relief model (MSRM): A new algorithm for the visualization of subtle topographic change of variable size in digital elevation models," *Earth Surface Processes Landforms*, vol. 43, no. 6, pp. 1361–1369, May 2018.

[166] G. Castelli, L. A. A. Oliveira, F. Abdelli, H. Dhaou, E. Bresci, and M. Ouessar, "Effect of traditional check dams (jessour) on soil and olive trees water status in Tunisia," *Sci. Total Environ.*, vol. 690, pp. 226–236, Nov. 2019.

[167] C. H. Wilson, T. T. Caughlin, S. W. Rifai, E. H. Boughton, M. C. Mack, and S. L. Flory, "Multi-decadal time series of remotely sensed vegetation improves prediction of soil carbon in a subtropical grassland," *Ecological Appl.*, vol. 27, no. 5, pp. 1646–1656, Jul. 2017.

[168] K. Ivushkin, H. Bartholomeus, A. K. Bregt, A. Pulatov, B. Kempen, and L. de Sousa, "Global mapping of soil salinity change," *Remote Sens. Environ.*, vol. 231, Sep. 2019, Art. no. 111260.

[169] H. A. Orengo and A. Garcia-Molsosa, "A brave new world for archaeological survey: Automated machine learning-based potsherd detection using high-resolution drone imagery," *J. Archaeological Sci.*, vol. 112, Dec. 2019, Art. no. 105013.

[170] H. Orengo and C. Petrie, "Large-scale, multi-temporal remote sensing of Palaeo-River networks: A case study from Northwest India and its implications for the Indus Civilisation," *Remote Sens.*, vol. 9, no. 7, Jul. 2017, Art. no. 735.

[171] B. Liss, M. D. Howland, and T. E. Levy, "Testing Google Earth Engine for the automatic identification and vectorization of archaeological features: A case study from Faynan, Jordan," *J. Archaeological Sci. Rep.*, vol. 15, pp. 299–304, Oct. 2017.

[172] F. J. Hasiuk, C. Harding, A. R. Renner, and E. Winer, "TouchTerrain: A simple web-tool for creating 3D-printable topographic models," *Comput. Geosci.*, vol. 109, pp. 25–31, Dec. 2017.

[173] M. B. Lyons *et al.*, "Monitoring large and complex wildlife aggregations with drones," *Methods Ecol. Evol.*, vol. 10, no. 7, pp. 1024–1035, Jul. 2019.

[174] F. Ascensão, D. Yogui, M. Alves, E. P. Medici, and A. Desbiez, "Predicting spatiotemporal patterns of road mortality for medium-large mammals," *J. Environ. Manage.*, vol. 248, Oct. 2019, Art. no. 109320.

[175] B. A. Wong, C. Thomas, and P. Halpin, "Automating offshore infrastructure extractions using synthetic aperture radar & Google Earth Engine," *Remote Sens. Environ.*, vol. 233, Nov. 2019, Art. no. 111412.

[176] A. Rasul, "An investigation into the location of the crashed aircraft through the use of free satellite images," *J. Photogrammetry Remote Sens. Geoinf. Sci.*, vol. 87, no. 3, pp. 119–122, Sep. 2019.

[177] J. Bian, A. Li, G. Lei, Z. Zhang, and X. Nan, "Global high-resolution mountain green cover index mapping based on Landsat images and Google Earth Engine," *ISPRS J. Photogrammetry Remote Sens.*, vol. 162, pp. 63–76, Apr. 2020.

[178] J.-F. Pekel, A. Cottam, N. Gorelick, and A. S. Belward, "High-resolution mapping of global surface water and its long-term changes," *Nature*, vol. 540, no. 7633, pp. 418–422, Dec. 2016.

[179] Q. Li, C. Qiu, L. Ma, M. Schmitt, and X. X. Zhu, "Mapping the land cover of Africa at 10 m resolution from multi-source remote sensing data with Google Earth Engine," *Remote Sens.*, vol. 12, no. 4, p. 602, Feb. 2020.
[180] P. Gong *et al.*, "Stable classification with limited sample: transferring a 30-m resolution sample set collected in 2015 to mapping 10-m resolution global land cover in 2017," *Sci. Bull.*, vol. 64, no. 6, pp. 370–373, Mar. 2019.
[181] A. E. Beresford, P. F. Donald, and G. M. Buchanan, "Repeatable and standardised monitoring of threats to key biodiversity areas in Africa using Google Earth Engine," *Ecol. Indic.*, vol. 109, Feb. 2020, Art. no. 105763.
[182] P. Teluguntla *et al.*, "A 30-m landsat-derived cropland extent product of Australia and China using random forest machine learning algorithm on Google Earth Engine cloud computing platform," *ISPRS J. Photogrammetry Remote Sens.*, vol. 144, pp. 325–340, Oct. 2018, doi: 10.1016/j.isprsjprs.2018.07.017.
[183] R. Goldblatt, W. You, G. Hanson, and A. Khandelwal, "Detecting the boundaries of urban areas in India: A dataset for pixel-based image classification in Google Earth Engine," *Remote Sens.*, vol. 8, no. 8, Aug. 2016, Art. no. 634.

Meisam Amani (Senior Member, IEEE) received the B.Eng. degree in geomatics engineering from the University of Tabriz, Tabriz, Iran, in 2012, the M.Eng. degree in remote sensing engineering from K.N. Toosi University of Technology, Tehran, Iran, in 2014, and the Ph.D. degree in electrical engineering from Memorial University of Newfoundland, St. John's, NL, USA, in 2018.

He is currently a Senior Remote Sensing Scientist and the Key Specialty Leader of Data Analytics at a global consulting and engineering company, called Wood plc, where he manages and leads various academic, governmental, and industrial remote sensing projects worldwide. He has worked on different applications of remote sensing, including but not limited to land cover/land use classification, soil moisture estimation, drought monitoring, water quality assessment, watershed management, power/transmission line monitoring, fog detection and nowcasting, and ocean wind estimation. To do these, he has utilized various remote sensing datasets and different machine learning and big data processing algorithms.

Dr. Amani is an Associate Editor in IEEE JSTARS and the lead guest editor for a special issue in the *Remote Sensing* journal. He also serves as a regular Reviewer in about 15 international remote sensing journals. A list of his research works can be found at https://www.researchgate.net/profile/Meisam_Amani3.

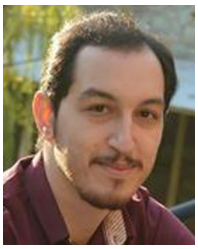

Arsalan Ghorbanian received the B.Sc. degree in geodesy and geomatics and the M.Sc. degree in remote sensing, in 2016 and 2018, respectively, from K. N. Toosi University of Technology, Tehran, Iran, where he is currently working toward the Ph.D. degree in remote sensing.

His research interests include land cover mapping, big data processing, image and video processing, soil moisture estimation from SAR data, and hyperspectral dimension reduction.

Seyed Ali Ahmadi received the B.Sc. and M.Sc. degrees from the Faculty of Geodesy and Geomatics, K. N. Toosi University of Technology, Tehran, Iran, where he is currently working toward the Ph.D. degree.

He worked on image classification and segmentation techniques, machine learning algorithms, and LiDAR data processing. His thesis was focused on classifying hyperspectral and LiDAR data sets by combining spectral and spatial features in order to increase the classification accuracy. His research interests include machine learning, deep learning, LiDAR data processing, hyperspectral image analysis, data fusion, image processing, and computer vision techniques.

Mohammad Kakooei received the B.S. degree from Shahid Beheshti University, Tehran, Iran, in 2011, the M.Sc. degree from Iran University of Science and Technology, Tehran, in 2014, and the Ph.D. degree in electronic engineering from Babol Noshirvani University of Technology (NIT), Babol, Iran, in 2020.

He is currently a Researcher with the Department of Computer & Electrical Engineering, NIT. His research interests include image processing, machine learning, remote sensing, parallel processing, GPGPU, CUDA, and data mining applications.

Armin Moghimi received the B.Sc. and M.Sc. degrees in photogrammetry and geomatics engineering from the K. N. Toosi University of Technology, Tehran, Iran, in 2013 and 2015, respectively. He is currently working toward the Ph.D. degree in photogrammetry and remote sensing at the K. N. Toosi University.

His research interests include change detection techniques, image preprocessing, image registration, and Lidar.

S. Mohammad Mirmazloumi (Student Member, IEEE) received the degree B.Sc. in geomatics from the University of Tabriz, Tabriz, Iran, in 2012, and the M.Sc. degree in remote sensing from K. N. Toosi University of Technology, Tehran, Iran, in 2015, where his research focused on retrieval of soil surface parameters using AIRSAR. She is currently working toward the Ph.D. degree in aerospace science and technology in the Polytechnic University of Catalonia, Barcelona, Spain.

He is currently a Research Assistant with the Remote Sensing Department, Centre Tecnològic de Telecomunicacions de Catalunya (CTTC). His research interests include SAR data applications, DInSAR, land cover classification, and soil surface parameters' retrievals.

Sayyed Hamed Alizadeh Moghaddam was born in 1994. He received the B.S. degree in survey engineering from the University of Isfahan, Isfahan, Iran, in 2016, and the M.Sc. degree in remote sensing from the Khajeh Nasir Toosi University of Technology, Tehran, Iran, in 2018.

His research interests include geometric processing of satellite images, hyperspectral remote sensing, dimensionality reduction, computational intelligence, and oil spill detection using SAR data.

Sahel Mahdavi received the Ph.D. degree in electrical engineering from Memorial University of Newfoundland, St. John's, NL, USA, in 2018.

Having almost ten years of academic background in *Remote Sensing*, she is familiar with a wide array of topics relevant to RS/GIS and their applications in various environmental aspects. These topics include object-based wetland classification using a combination of optical and full-polarimetric SAR data, feature selection, soil moisture retrieval using SAR images, image segmentation, speckle reduction in SAR images, target detection in multispectral optical images, and the relationship between environmental conditions and SAR images. She also coauthored a book entitled *Principles of SAR Remote Sensing*. She has authored more than 25 journals. She was a member of a provincial project on wetland classification during her Ph.D. when she identified the problem with wetland classification using *Remote Sensing* and, subsequently, proposed a novel scheme for wetland mapping. She is currently affiliated with the Data Analytics team at Wood PLC.

Dr. Mahdavi was the recipient of the Newfoundland and Labrador Branch of Canadian Institute of Geomatics Scholarship (2015) and the Emera Graduate Scholarship for Distinctive Women in Engineering for three consecutive years (2016–2018).

Masoud Ghahremanloo received the B.S. degree in geodesy and geomatics from Zanjan University, Zanjan, Iran, in 2012, and the M.S. degree in remote sensing from K.N. Toosi University of Technology, Tehran, Iran, in 2018. He is currently working toward the Ph.D. degree in Earth and atmospheric sciences from the University of Houston, Houston, TX, USA.

His research interests include satellite remote sensing and application of artificial intelligence, machine learning (ML), and deep learning (DL) in study of Earth and atmosphere. He is actively involved with ML/DL algorithm development and scientific data utilization of different satellite remote sensing missions.

Saeid Parsian received the B.Eng. degree in geomatics engineering from the University of Tabriz, Tabriz, Iran, in 2012, and the M.Eng. degree in photogrammetry from Tafresh University, Tehran, Iran, in 2015.

He has extensive work experience as a surveying operator, and has contributed to several civil and surveying projects, such as road and tunnel design, land registration, and satellite image processing and analysis. His current research interests include utilizing multisource remote sensing datasets for flood mapping and risk assessment.

Qiusheng Wu received the Ph.D. degree in geography from the University of Cincinnati, Cincinnati, OH, USA, in 2015.

He is currently an Assistant Professor with the Department of Geography, University of Tennessee, Knoxville, TN, USA. His research interests include remote sensing, open-source GIS, wetland hydrology, and Google Earth Engine.

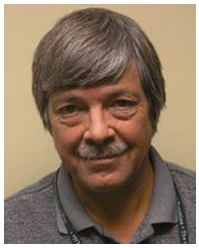

Brian Brisco received the B.Sc. degree in ecology and the M.Sc. degree in soil science both from the University of Guelph, Guelph, ON, Canada, in 1977 and 1981, respectively. He also received the Ph.D. degree in remote sensing/physical geography from the University of Kansas, Lawrence, KS, USA, in 1985.

He is an internationally recognized authority on Synthetic Aperture Radar (SAR) and its application to a wide range of environmental monitoring applications. He has been involved in remote sensing since 1975 and participated in the SURSAT project from 1977 to 1980 before spending 4 years at the Remote Sensing Laboratory at the University of Kansas under the supervision of Dr. F.T. Ulaby, widely recognized as one of the world's leading authorities on radar. He worked for Intera from 1989 until 1997 as a Research Associate after completion of an NSERC Postdoctoral fellowship served at the Canada Centre for Remote Sensing. From 1997 to 2004 he worked for Noetix Research Inc., where he was the Director of Research and Applications Development. In 2004, he joined CCRS as a Research Scientist. His research activities focus on using remote sensing, particularly synthetic aperture radar (SAR), for mapping and managing renewable resources. His extensive publications include studies on vegetation characterization, crop identification and monitoring, conservation farming/ soil erosion mapping, soil moisture estimation, land cover mapping, wetland mapping, rangeland management, forestry, and developing tools, and techniques for ground truth data acquisition. His work has included experience with interferometry, polarimetry, and radar backscatter modeling including software development and operational implementation. He has authored or coauthored more than 200 publications including more than 50 peer-reviewed journal publications and is the author of two chapters in the *Manual of Remote Sensing* volume on radar applications published by ASPRS. He provides peer review services to all the major remote sensing journals and participates as an external examiner for many graduate students at various universities in Canada and abroad. He has been consulted or contracted by government and non-government organizations on a wide range of SAR applications and system development including NRCan, CSA, DND, AAFC, EC, NASA, ESA, NASDA, NOAA, USDA, CAS, etc. He has extensive contacts in the SAR community worldwide and has worked in China, Vietnam, Malaysia, Thailand, Indonesia, South Africa, Argentina, Uruguay, Chile, Brazil, Columbia, and Costa Rica.

Dr. Brisco is a Past-President of the Canadian Remote Sensing Society (CRSS) and the Canadian Aeronautics and Space Institute.